Physica Scripta

PAPER

On interplay of surface tension and inertial stabilization mechanisms in the stable and unstable interface dynamics with the interfacial mass flux

RECEIVED
17 December 2020

REVISED
26 March 2021

ACCEPTED FOR PUBLICATION
7 April 2021

PUBLISHED
12 May 2021

D V Ilyin[1], W A Goddard III[1], I I Abarzhi[3] and S I Abarzhi[2,*]

[1] California Institute of Technology, Pasadena, CA 91125, United States of America
[2] The University of Western Australia, Crawley, Perth, WA 6009, Australia
[3] Institute for Engineering Thermophysics, National Academy of Sciences, Kiev, 03057, Ukraine
[*] Author to whom any correspondence should be addressed.

E-mail: snezhana.abarzhi@gmail.com

Keywords: interfacial mixing, non-equilibrium dynamics, fluid instability, dynamics of fluids, dynamics of plasmas, dynamics of materials

Abstract

Non-equilibrium dynamics of interfaces and mixing are omnipresent in fluids, plasmas and materials, in nature and technology, at astrophysical and at molecular scales. This work investigates dynamics of an interface separating fluids of different densities and having interfacial mass flux, and being influenced by the acceleration and the surface tension. We derive solutions for the interface dynamics conserving mass, momentum and energy, find the critical acceleration values separating stable and unstable regimes, and reveal the macroscopic inertial mechanism as primary mechanism of the interface stabilization. We show that while the surface tension influences only the interface, its presence leads to formation of vortical structures in the bulk. For large accelerations the conservative dynamics is unstable, leading to the growth of interface perturbations and the growth of the interface velocity. This new instability can be unambiguously discerned from other instabilities; for strong accelerations it has the fastest growth-rate and the largest stabilizing surface tension value when compared to Landau-Darrieus and Rayleigh-Taylor instabilities. We further find the values of initial perturbation wavelengths at which the conservative dynamics can be stabilized and at which it has the fastest growth. Our results agree with existing observations, identify extensive theory benchmarks for future experiments and simulations, and outline perspectives for application problems in nature and technology.

1. Introduction

Non-equilibrium transport, interfaces and mixing are omnipresent in nature and technology at astrophysical and at molecular scales, and in high and low energy density regimes [1]. Thermonuclear flashes on the surface of compact stars, the fingering of the interstellar medium along the edge of a black hole, the formation of hot spot in inertial confinement fusion, the particle-field interactions in imploding Z-pinches, the coronal mass ejections in the Solar flares, the plasma instabilities in the Earth ionosphere, the deep ocean convection events in the polar region, the pollutant dispersion in the atmosphere, plasma thrusters, nano-fabrication, fossil fuel extraction, and premixed combustion – are examples of processes governed by the non-equilibrium interfacial dynamics [2–19]. These realistic environments are often characterized by sharply and rapidly changing flow fields and by small effects of dissipation and diffusion, which result in the formation of discontinuities (referred to as fronts or as interfaces) between the flow non-uniformities (phases) at macroscopic (continuous) scales [11]. Non-equilibrium dynamics of interfaces and mixing are challenging to study in their direct manifestations in theory, experiment and simulations, and are a source of paradigm shifts in science, mathematics and engineering [1, 2, 18].

In this work we systematically investigate the dynamics of the interface that separates fluids of different densities, has the interfacial mass flux, and is influenced by the acceleration and the surface tension [20]. Through the general theoretical framework [21–23], we derive solutions for the interface dynamics conserving

mass, momentum and energy, find the critical acceleration values separating stable and unstable regimes, and reveal the macroscopic inertial mechanism as primary mechanism of the interface stabilization. We show that while the surface tension influences only the interface, its presence leads to formation of vortical structures in the bulk. For large accelerations the dynamics is unstable, leading to the growth of the interface perturbations and the growth of the interface velocity. This instability of the conservative dynamics can be unambiguously discerned from other fluid instabilities.

The paper is organized as follows. Following the Introduction in section 1, we provide the Method in section 2, including the governing equation (2.1), the theoretical approach (2.2), and the fundamental solutions (2.3). We present in section 3 the Results of our analysis for the conservative dynamics, and for the dynamics of the Landau-Darrieus and Rayleigh-Taylor instabilities influenced by the acceleration and the surface tension. This includes the fundamental solutions (3.1), the systematic study of the properties of the inertial dynamics free from surface tension (3.2) and with surface tension (3.3), the focused analyses of the accelerated dynamics free from surface tension (3.4) and with surface tension (3.5), the investigations of the mechanisms of the interface stabilization and destabilization (3.6) and the characteristic scales (3.7), as well as the theory outcomes for experiments and simulations (3.8). We finalize the work with Discussion in section 4, and provide Acknowledgements, Data availability, Author's contributions, References, Tables, and Figure captions and Figures in sections 5–10.

When looking from a far field, an observer ordinarily considers two kinds of discontinuities separating the flow phases: a front and an interface [20]. The front has zero mass flux across it. Through the interface the mass can be transported. The fluid phases are broadly defined: These can be the distinct kinds of matter or the same kind of matter with distinct thermodynamic properties. To describe the multi-phase flow, a boundary value problem should be solved by balancing the fluxes of mass, momentum and energy at a freely evolving discontinuity. While the boundary value problems are challenging to investigate, this approach has a number of advantages, and the boundary value problem solution has high predictive capability in a broad parameter regime [21].

The unstable accelerated fronts are represented by Rayleigh-Taylor and Richtmyer-Meshkov instabilities [24–27]. The fundamental properties of Rayleigh-Taylor and Richtmyer-Meshkov dynamics in the scale-dependent early-time and late-time regimes and in the self-similar interfacial mixing regime are well captured by the group theory approach and by the linear and weakly nonlinear theories [28–31]. For interfaces, the classical theoretical framework for the problem was developed by Landau [32]. It considered the dynamics of ideal incompressible fluids, balanced at the interface the fluxes of mass and momentum and postulated the special condition for the perturbed mass flux [32]. Several seminal models further connected this framework to realistic environments in high energy density plasmas and in reactive and super-critical fluids [33–38].

The dynamics of interfaces with interfacial mass flux is a long-standing problem in science, mathematics and engineering [1]. It has wide-ranging applications in plasmas (dynamics of ablation front influencing the hot spot formation in inertial confinement fusion), astrophysics (thermonuclear flashes determining the nuclear synthesis in type-Ia supernova), material science (material transformations under high strain rates in nano-fabrication), and industry (scramjets) [1, 2]. To tackle these research frontiers and to solve a broad class of problems, the theory of interface dynamics was recently developed [21–23].

This theory elaborated the general framework for the problem of the interface stability, directly linked the microscopic transport at the interface to macroscopic fields in the fluids' bulk, and reported the mechanisms of the interface stabilization and destabilization never previously discussed [21–23]. The key discoveries – the inertial mechanism of the interface stabilization, the new fluid instability of the accelerated interface, and the chemistry-induced instabilities – identified the fundamental properties of the interface dynamics. They also resolved the long-standing prospect of Landau [32], by showing that the classical Landau's solution for Landau-Darrieus instability is a perfect mathematical match [21–23].

The theory [21–23] considered the inertial and the accelerated interface dynamics for ideal incompressible fluids free from stabilizations caused by interactions of particles at molecular scales [14–17]. Realistic processes are usually accompanied by dissipation, diffusion, compressibility, radiation transport, stratification, surface tension and other effects [3–15, 39–43]. The influence of these effects on the interface dynamics call for systematic investigations [21].

Here we study the interface dynamics with interfacial mass flux in the presence of acceleration and surface tension. The fluids are ideal and incompressible, with negligible stratification and densities variation, the flow is two-dimensional, periodic and spatially extended. The destabilizing acceleration is directed from the heavy to the light fluid. Macroscopically, the surface tension is understood as a tension at the phase boundary between the flow phases [20, 21]. Microscopically, the surface tension is caused by anisotropy of interactions between the particles near the interface which results in energy consumption with the increasing interface area [14, 20, 41]. Physically, the surface tension is always present in a multiphase flow. Mathematically, the surface tension is accounted for through the pressure modification in the governing equations [14, 20, 21]. We investigate the

interplay of the macroscopic and microscopic stabilizations due to the inertial effect and surface tension, respectively, with the destabilizing acceleration in the interface dynamics with interfacial mass flux.

In order to address this task, we advance and employ the general method [21, 22] to rigorously solve the linearized boundary value problem conserving mass, momentum and energy. We find that depending on the acceleration and the surface tension, the dynamics can be stable or unstable. In the stable regime, the flow may have non-perturbed flow fields in the bulk and a constant interface velocity. The conservative dynamics is unstable only when it is accelerated and when the acceleration value exceeds a threshold. This threshold value combines the contributions of the inertial and the surface tension mechanisms and is finite for zero surface tension. The unstable dynamics couples the interface perturbations with the potential and vortical components of the velocity fields in the fluids' bulk and is shear free at the interface. It describes the standing wave with the growing amplitude, and has the growing interface velocity. This instability of the conservative dynamics has unique quantitative and qualitative properties unambiguously differentiating it from other fluid instabilities. Particularly, it has the fastest growth-rate and the largest stabilizing surface tension value in the extreme regime of strong accelerations, when compared to the Landau-Darrieus and Rayleigh-Taylor instabilities. We further find the critical and maximum values of the initial perturbation wavelengths at which the fluid instability of the conservative dynamics can be stabilized and at which its growth is the fastest. Based on the obtained results, we identify the theory benchmarks for future experiments and simulations and for application problems in nature and technology [1–15, 39–45].

The problem of the interface dynamics with the interfacial mass flux is a corner-stone problem of physics, mathematics and engineering [1, 2]. On the side of physics, one needs to grasp non-equilibrium dynamics of interfaces and mixing in order to better understand a broad range of natural phenomena, from celestial events to molecules [3–10]. On the side of mathematics, this problem is even more challenging than the Millennium problem of the Navier-Stokes equation, since, in addition to solution of nonlinear partial differential equations in the bulk, it requires a solution of a boundary value problem at an unstable freely evolving interface and an ill-posed initial value problem [1, 18–23, 46, 47]. In engineering, the multiphase flows are critical to technological and industrial processes, including nano-fabrication, gas and oil extraction, and purification of water [11–17]. Hence, the problem studied in this paper - the interface dynamics with interfacial mass flux - fits naturally into the scope of Physica Scripta and the Focus Issue 'Turbulent Mixing and Beyond' [48].

The problem solution requires one to develop a rigorous and general theory applicable in a broad range of conditions [20–23, 46]. It also demands the elucidation of the so-called third prospect of Landau – the 1962 Noble Laureate and one of founders of modern theoretical physics [20]. The resolutions of the two other prospects of Landau – the theory of phase transitions and the theory of superconductors – were recognized with Noble prizes in 1982 and 2003 [20, 49]. Our theoretical approach enables a rigorous, general and systematic treatment of the interface dynamics, and finds that the classical Landau's solution for the Landau-Darrieus instability is a perfect mathematical match requiring energy imbalance at the interface [21–23, 46]. Our first work on the subject [23] was selected by Physica Scripta as Research Highlight [50].

Our theoretical approach reveals the physics of the interface dynamics through the analysis of mathematical attributes of rigorous analytical solutions, including, e.g., the direct link of the properties of macroscopic fields in the bulk to microscopic transport at the interface, the inertial stabilization mechanism, and the new fluid instability [21–23, 46]. It calls for further systematic developments, including, e.g., the theory of ablative Rayleigh-Taylor instability in fusion plasmas, the theory of D'yakov-Kontorovich instability of shock waves, and the bridge of the concepts of the linear response theory, self-similarity and interfaces [20–23, 46]. The present work studies the interface dynamics and focuses on the interplay of the destabilizing acceleration with macroscopic and microscopic stabilizations due to the inertial effect and the surface tension, respectively, in the interface dynamics with the interfacial mass flux.

2. Method

2.1. Governing equations

Conservation laws: In the inertial frame of reference, the dynamics of ideal fluid is governed by the conservation of mass, momentum, and energy as

$$\frac{\partial \rho}{\partial t}+\frac{\partial \rho v_i}{\partial x_i}=0,\quad \frac{\partial \rho v_i}{\partial t}+\frac{\partial \rho v_i v_j}{\partial x_j}+\frac{\partial P}{\partial x_i}=0,\quad \frac{\partial E}{\partial t}+\frac{\partial (E+P)v_i}{\partial x_i}=0 \tag{1}$$

Here x_i are the spatial coordinates, $(x_1, x_2, x_3) = (x, y, z)$, t is time, $(\rho, \mathbf{v}, P, E)$ are the fields of density ρ, velocity $\mathbf{v}$, pressure P and energy density E, and e is specific internal energy [20–23]. The inertial frame of reference is referred to the frame of reference moving with constant velocity $\tilde{\mathbf{V}}_0$ relative the laboratory frame of

reference; for definiteness $\tilde{\mathbf{V}}_0 = (0,\ 0,\ \tilde{V}_0)$ [21, 22]. The governing equations equation (1) are augmented with the closure equation – the equation of state associating the internal energy and pressure [20].

For a system of two fluids with different densities separated by an interface, we mark the fields of the heavy (light) fluid as $(\rho,\ \mathbf{v},\ P,\ E)_{h(l)}$, and we introduce a continuous local scalar function $\theta(x,\ y,\ z,\ t)$ to describe the interface. The function value is $\theta = 0$ at the interface and it is $\theta > 0$ ($\theta < 0$) in the heavy (light) fluid [21–23, 28, 29]. By using the Heaviside step-function $H(\theta)$ we represent the flow fields in the entire domain as $(\rho,\ \mathbf{v},\ P,\ E) = (\rho,\ \mathbf{v},\ P,\ E)_h H(\theta) + (\rho,\ \mathbf{v},\ P,\ E)_l H(-\theta)$ [18, 19, 21–23].

Boundary value problem: At the interface, the balance of fluxes of mass and normal and tangential components of momentum and energy obey the boundary conditions [21–23, 28, 29]:

$$[\tilde{\mathbf{j}}\cdot\mathbf{n}] = 0,\quad \left[\left(P + \frac{(\tilde{\mathbf{j}}\cdot\mathbf{n})^2}{\rho}\right)\mathbf{n}\right] = 0,\quad \left[\frac{(\tilde{\mathbf{j}}\cdot\mathbf{n})(\tilde{\mathbf{j}}\cdot\boldsymbol{\tau})}{\rho}\boldsymbol{\tau}\right] = 0,\quad \left[(\tilde{\mathbf{j}}\cdot\mathbf{n})\left(W + \frac{\tilde{\mathbf{j}}^2}{2\rho^2}\right)\right] = 0 \qquad (2)$$

where the jump of functions across the interface is denoted with [...]; the unit vectors normal and tangential at the interface are $\mathbf{n}$ and $\boldsymbol{\tau}$ with $\mathbf{n} = \nabla\theta/|\nabla\theta|$ and $(\mathbf{n}\cdot\boldsymbol{\tau}) = 0$; the mass flux across the moving interface is $\tilde{\mathbf{j}} = \rho(\mathbf{n}\dot{\theta}/|\nabla\theta| + \mathbf{v})$; the specific enthalpy is $W = e + P/\rho$ [21–23, 28, 29].

The boundary conditions at the interface equation (2) are derived directly from the conservation laws in the bulk equation (1) in the inertial frame of reference. They are exact and are independent of the velocity $\tilde{\mathbf{V}}_0$ of the inertial frame of reference [21]. This general formulation allows us to stay free from traditional postulate of the constancy of interface velocity [20], and to examine the sensitivity of the dynamics to the boundary conditions at the interface, including the flow fields' structure and the interface stability [46].

We consider the spatially extended flow, which is unbounded in the z direction and is periodic in the $(x,\ y)$ plane. The heavy (light) fluid is located in the lower (upper) sub-domain. The boundary conditions at the outside boundaries of the domain are

$$\mathbf{v}_h|_{z\to-\infty} = \mathbf{V}_h = (0,\ 0,\ V_h),\qquad \mathbf{v}_l|_{z\to+\infty} = \mathbf{V}_l = (0,\ 0,\ V_l) \qquad (3)$$

with the constant velocity magnitude(s) $V_{h(l)}$, figure 1.

Interface velocity: The interface velocity in the laboratory frame of reference is $\tilde{\mathbf{V}}$. For the steady planar interface normal to the mass flux, the interface velocity is constant; this velocity can be chosen equal to the velocity of the inertial frame of reference as $\tilde{\mathbf{V}}_0 = \tilde{\mathbf{V}}$. For the non-steady non-planar interface arbitrarily positioned relative to the mass flux, the interface velocity $\tilde{\mathbf{V}}$ and the velocity of the inertial frame of reference $\tilde{\mathbf{V}}_0$ are distinct, $\tilde{\mathbf{V}} \neq \tilde{\mathbf{V}}_0$ [21]. In this general case, the interface velocity $\tilde{\mathbf{V}}$ obeys the relation

$$\tilde{\mathbf{V}}n = -\mathbf{v}\mathbf{n}|_{\theta=0} = -(\tilde{\mathbf{j}}/\rho)\mathbf{n}|_{\theta=0} \qquad (4)$$

Flow configuration: The flow is subject to the acceleration and the interfacial surface tension. The acceleration $\mathbf{g}$ is directed along the z direction from the heavy fluids to the light fluid, as $\mathbf{g} = (0,\ 0,\ g),\quad g \geqslant 0$. The interfacial surface tension is understood as the tension between the fluid phases, and is characterized by the surface tension coefficient $\sigma,\quad \sigma \geqslant 0$.

We consider a sample case of a two-dimensional flow periodic in the x direction, free from motion in the y direction and spatially extended in the z direction. The interfacial function θ is set as

$$\theta = -z + z^*(x,\ t),\qquad \dot{\theta} = \frac{\partial z^*}{\partial t},\qquad \nabla\theta = \left(\frac{\partial z^*}{\partial x},\ 0,\ -1\right),\qquad |\nabla\theta| = \sqrt{1 + \left(\frac{\partial z^*}{\partial x}\right)^2} \qquad (5)$$

Figure 1 illustrates the schematics of the dynamics in equations (1)–(5) in a far field (not to scale). The heavy (light) fluid with the density $\rho_{h(l)}$ is located in the lower (upper) part of the domain and has the uniform velocity field $\mathbf{V}_{h(l)} = (0,\ 0,\ V_{h(l)})$ marked by arrows far from the interface. Blue color marks the interface between the fluids with solid (dashed) line for the perturbed (planar) interface. The acceleration $\mathbf{g} = (0,\ 0,\ g),\quad g \geqslant 0$ is directed from the heavy to the light fluid and is along the z-direction. In this configuration the gradients of the pressure and density are directed oppositely, and the acceleration destabilizes the dynamics; the case of zero mass flux corresponds to Rayleigh-Taylor instability (RTI). The surface tension $\sigma,\quad \sigma \geqslant 0$ is present at the interface. The flow is two-dimensional.

Some discussion is required on nature of the acceleration [18–30]. The acceleration can destabilize the dynamics when the gradients of pressure and density are directed oppositely [24–27]. This can occur when the flow is a subject to acceleration directed from the heavy to the light fluid and the acceleration is due the body force. This can also occur when the fluid interface moves with the acceleration directed from the light to the heavy fluid [24–27, 51]. The former case is illustrated by water flowing from an overturned cup under the influence of gravity [24, 51]. The latter case is observed in experiments in shock-driven fluids and plasmas [18, 25–28, 52, 53]. For a nearly planar interface with zero interfacial mass flux, as in early-time Rayleigh-Taylor instability, these definitions are equivalent, because the interface dynamics can be considered in a non-inertial

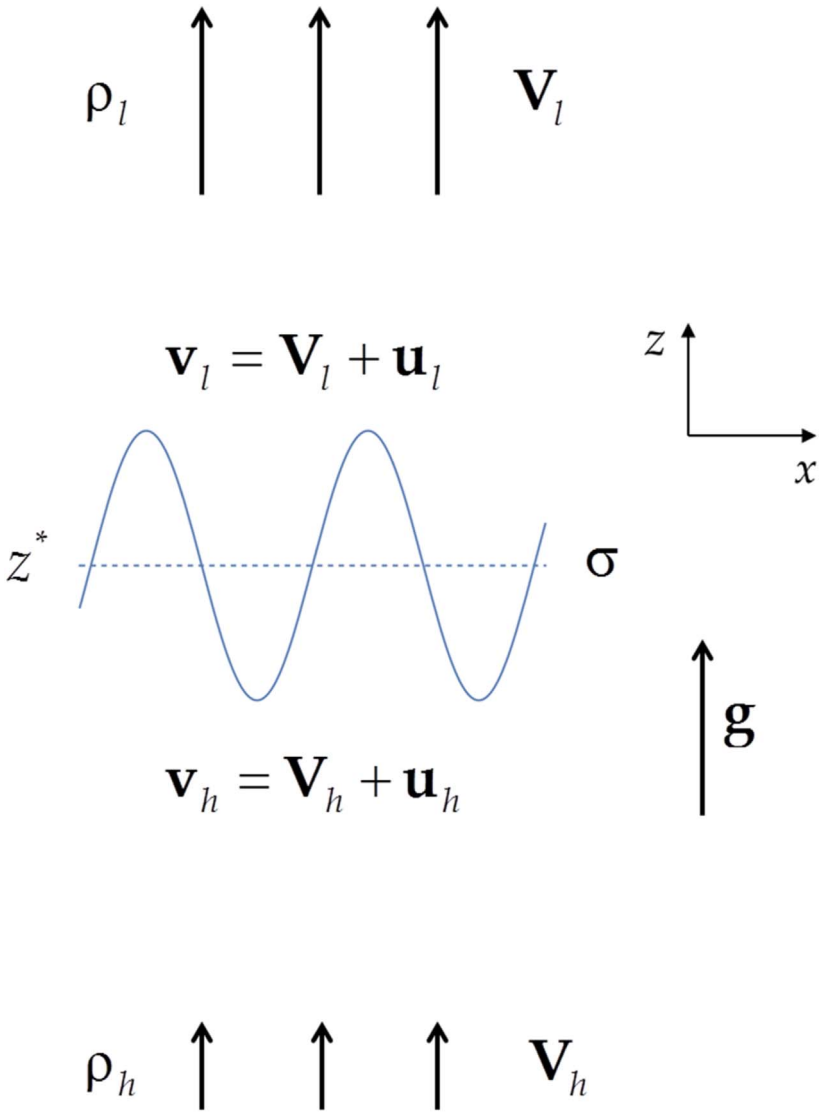

Figure 1. Schematics of the dynamics in a far field (not to scale). Blue color marks the planar (dashed line) interface and the perturbed (solid line) interface.

frame of reference moving with the accelerated interface [24–28]. In general case of an unsteady non-planar interface with interfacial mass flux, the former definition is usually applied [18–22, 29–38]. In our theory we consider the dynamics of the fluids and their interface in the inertial frame of reference, when the acceleration is due to the body force and is directed from the heavy to the light fluid.

In schematics of acceleration-driven instabilities and RTI in the literature [18, 19, 28–30], it is usual that the acceleration is against the z direction and the heavy (light) fluid is located in the upper (lower) part of the domain. Such configuration refers to our everyday experience when we observe RTI by watching water flowing from an overturned cup [28–30]. For the purposes of the present paper, we keep the direction of the acceleration from the heavy to the light fluid, and we locate the heavy (light) fluid in the lower (upper) part of the domain. This configuration is free from the loss of generality and from the influencing the results [21, 22]. The configuration is used because for the interface dynamics with the interfacial mass flux, the velocity field of the heavy fluid is potential whereas the velocity field of the light fluid is a superposition of the potential and vortical components, see section 2.3 for details [20–23, 32–38, 46]. The flow configuration as in figure 1 allows us to better illustrate the light fluid flow fields of and to easier compare the flow fields of the conservative dynamics with interfacial mass flux with those of Landau-Darrieus and Rayleigh-Taylor instabilities, see figures 3, 6–9 [20–23, 32–38, 46].

2.2. Linearized dynamics

The governing equations equations (1)–(4) are extremely challenging. They can be simplified by the conditions of small perturbations, mass flux directionality and incompressibility.

Dynamics perturbations: The unperturbed flow fields are uniform, $\{\tilde{\mathbf{j}},\ \mathbf{v},\ P,\ W\} = \{\mathbf{J},\ \mathbf{V},\ P_0,\ W_0\}$, the unperturbed interface is planar, and the normal and tangential unit vectors of the unperturbed interface are $\{\mathbf{n},\ \boldsymbol{\tau}\} = \{\mathbf{n}_0,\ \boldsymbol{\tau}_0\}$ equation (2). We slightly perturb in equations (1)–(4) the flow fields as $\tilde{\mathbf{j}} = \mathbf{J} + \mathbf{j}$, $\mathbf{v} = \mathbf{V} + \mathbf{u}$, $P = P_0 + p$, and $W = W_0 + w$, with $|\mathbf{j}| \ll |\mathbf{J}|$, $|\mathbf{u}| \ll |\mathbf{V}||p| \ll |P_0|$ and $|w| \ll |W_0|$. We slightly perturb the fluid interface as $\mathbf{n} = \mathbf{n}_0 + \mathbf{n}_1$ and $\boldsymbol{\tau} = \boldsymbol{\tau}_0 + \boldsymbol{\tau}_1$, with $|\mathbf{n}_1| \ll |\mathbf{n}_0|$ and $|\boldsymbol{\tau}_1| \ll |\boldsymbol{\tau}_0|$, and with $|\dot{\theta}/|\nabla\theta|| \ll |\mathbf{V}|$. The fluid density is perturbed as $\rho \to \rho + \delta\rho$ with $|\delta\rho| \ll |\rho|$. The perturbed velocity of the interface is $\tilde{\mathbf{V}} = \tilde{\mathbf{V}}_0 + \tilde{\mathbf{v}}$, with $|\tilde{\mathbf{v}}| \ll |\tilde{\mathbf{V}}_0|$.

To the leading order in small perturbations, the boundary conditions at the interface are:

$$[\mathbf{J}\cdot\mathbf{n}_0] = 0,\ \left[\left(P_0 + \frac{(\mathbf{J}\cdot\mathbf{n}_0)^2}{\rho}\right)\mathbf{n}_0\right] = 0,\ \left[(\mathbf{J}\cdot\mathbf{n}_0)\frac{(\mathbf{J}\cdot\boldsymbol{\tau}_0)}{\rho}\boldsymbol{\tau}_0\right] = 0,\ \left[(\mathbf{J}\cdot\mathbf{n}_0)\left(W_0 + \frac{\mathbf{J}^2}{2\rho^2}\right)\right] = 0 \tag{6.1}$$

To the first order, the boundary conditions at the interface are:

$$[\mathbf{j}\cdot\mathbf{n}_0 + \mathbf{J}\cdot\mathbf{n}_1] = 0,\quad \left[\left(p + \frac{2(\mathbf{J}\cdot\mathbf{n}_0)}{\rho}\left((\mathbf{j}\cdot\mathbf{n}_0 + \mathbf{J}\cdot\mathbf{n}_1) - \frac{(\mathbf{J}\cdot\mathbf{n}_0)}{2}\frac{\delta\rho}{\rho}\right)\right)\mathbf{n}_0\right] = 0,$$
$$\left[((\mathbf{J}\cdot\mathbf{n}_0)(\mathbf{J}\cdot\boldsymbol{\tau}_1 + \mathbf{j}\cdot\boldsymbol{\tau}_0) + (\mathbf{J}\cdot\boldsymbol{\tau}_0)(\mathbf{J}\cdot\mathbf{n}_1 + \mathbf{j}\cdot\mathbf{n}_0))\frac{\boldsymbol{\tau}_0}{\rho}\right] = 0,$$
$$\left[(\mathbf{J}\cdot\mathbf{n}_0)\left(w + \frac{(\mathbf{J}\cdot\mathbf{j})}{\rho^2} - \left(\frac{\delta\rho}{\rho}\right)\frac{\mathbf{J}^2}{\rho^2}\right)\right] = 0 \tag{6.2}$$

The small perturbations of the flow fields decay away from the interface:

$$\{\mathbf{j},\ \mathbf{v},\ p,\ w,\ \delta\rho\}_h|_{z\to-\infty} = 0,\ \{\mathbf{j},\ \mathbf{v},\ p,\ w,\ \delta\rho\}_l|_{z\to+\infty} = 0 \tag{6.3}$$

Physics assumptions: The boundary conditions in equations (2)–(4) and (6) are valid for compressible and incompressible ideal fluids, for two- and three-dimensional flows, and for arbitrary positioning of the interface relative the mass flux. Conditions equation (6) can be further simplified by applying the conditions of directionality of the mass flux, the incompressibility of the fluids, and the dimensionality of the flow.

Boundary conditions: Indeed, to the leading order, the mass flux is $\mathbf{J} = \rho\mathbf{V}$, the flow fields are uniform in the bulk, $(\rho,\ \mathbf{v},\ P,\ W)_{h(l)} = (\rho,\ \mathbf{V},\ P_0,\ W_0)_{h(l)}$, and obey conditions equation (3) at the boundaries of the domain. The components of mass flux normal and tangential to the interface are $J_n = \mathbf{J}\cdot\mathbf{n}_0$, $J_\tau = \mathbf{J}\cdot\boldsymbol{\tau}_0$. We presume that to the leading order the mass flux is normal to the planar interface; hence, its tangential component is zero, $J_\tau = 0$. In the limiting case of incompressible dynamics, the values approach $(P_0 + J_n^2/\rho)_{h(l)} \to (P_0)_{h(l)}$ and $(W_0 + \mathbf{J}^2/2\rho^2)_{h(l)} \to (W_0)_{h(l)}$, since the speed(s) of sound in the fluid(s) is substantially greater than other velocity scales. These transform equation (6.1) to

$$[J_n] = 0,\quad [P_0\ \ \mathbf{n}_0] = 0,\quad [J_n\ \ W_0] = 0 \tag{7}$$

For a two-dimensional flow in equation (5), to the leading order the normal and tangential vectors of the interface are $\mathbf{n}_0 = (0,\ 0,\ -1)$ and $\boldsymbol{\tau}_0 = (1,\ 0,\ 0)$. The first order perturbations of the normal and tangential vectors of the interface are $\mathbf{n}_1 = (\partial z^*/\partial x,\ 0,\ 0)$ and $\boldsymbol{\tau}_1 = (0,\ 0,\ \partial z^*/\partial x)$. This leads to $\mathbf{J}\cdot\mathbf{n}_1 = 0$. For incompressible fluids with negligible density perturbations $|\delta\rho/\rho| \ll |\mathbf{u}|/|\mathbf{V}|$ the first order boundary conditions at the interfaces equation (6.2) are then transformed to

$$[\mathbf{j}\cdot\mathbf{n}_0] = 0,\quad \left[\left(\left(p + \frac{2(\mathbf{J}\cdot\mathbf{n}_0)}{\rho}\right)(\mathbf{j}\cdot\mathbf{n}_0)\right)\mathbf{n}_0\right] = 0,$$
$$\left[(\mathbf{J}\cdot\mathbf{n}_0)\frac{(\mathbf{J}\cdot\boldsymbol{\tau}_1 + \mathbf{j}\cdot\boldsymbol{\tau}_0)}{\rho}\boldsymbol{\tau}_0\right] = 0,\quad \left[(\mathbf{J}\cdot\mathbf{n}_0)\left(w + \frac{(\mathbf{J}\cdot\mathbf{j})}{\rho^2}\right)\right] = 0 \tag{8.1}$$

The normal and tangential components of the perturbed mass flux are $j_n = \mathbf{j}\cdot\mathbf{n_0}$ and $j_\tau = \mathbf{j}\cdot\boldsymbol{\tau_0}$. In ideal incompressible fluids the internal energy is constant, $e = e_0$, and the perturbed enthalpy is $w = p/\rho$. The perturbed flow fields in the bulk and at the outside boundaries obey the equations [20–23]:

$$\nabla\cdot\mathbf{u} = 0,\quad \dot{\mathbf{u}} + (\mathbf{V}\cdot\nabla)\mathbf{u} + \frac{\nabla p}{\rho} = 0 \tag{8.2}$$

where the fields $(\rho,\ \mathbf{V},\ \mathbf{u},\ p)$ are $(\rho,\ \mathbf{V},\ \mathbf{u},\ p)_{h(l)}$ in the bulk of the heavy (light) fluid. The boundary conditions for the perturbed flow fields away from the interface are:

$$\mathbf{u}_h|_{z\to-\infty} = 0,\quad \mathbf{u}_l|_{z\to+\infty} = 0 \tag{8.3}$$

The interface velocity is $\tilde{\mathbf{V}} = \tilde{\mathbf{V}}_0 + \tilde{\mathbf{v}}$, with $|\tilde{\mathbf{v}}| \ll |\tilde{\mathbf{V}}_0|$. Up to the first order it is

$$\tilde{\mathbf{V}} = \tilde{\mathbf{V}}_0 + \tilde{\mathbf{v}}, \quad \tilde{\mathbf{v}}\mathbf{n}_0 = -(\mathbf{u}\cdot\mathbf{n}_0 + \dot{\theta}) \ |_{\theta=0} \tag{8.4}$$

To conclude this Sub-Section, we emphasize that, in excellent agreement with the classical results, for the interface dynamics with the interfacial mass flux, the tangential component of the velocity is continuous at the interface, with $[\mathbf{v}\cdot\boldsymbol{\tau}] = 0$, including the zeroth order $[\mathbf{V}\cdot\boldsymbol{\tau}_0] = 0$ and the first order $[\mathbf{V}\cdot\boldsymbol{\tau}_1 + \mathbf{u}\cdot\boldsymbol{\tau}_0] = 0$, and the velocity field is shear-free at the interface equations (2), (6), (8) [20–23, 46].

2.3. Fundamental solutions

Structure of solutions: We seek solutions for the boundary value problem equation (8) in which the perturbed velocity of the heavy fluid is potential in accordance with the Kelvin theorem, and the perturbed velocity of the light fluid has both potential and vortical components [20–23]:

$$\mathbf{u}_h = \nabla\Phi_h, \quad \mathbf{u}_l = \nabla\Phi_l + \nabla\times\boldsymbol{\Psi}_l \tag{9.1}$$

This structure of the solution agrees with observations and is established for any initial conditions [20].

The fluid potential and vortical fields and the interface perturbation are

$$\begin{gathered}\Phi_h = \Phi\exp(ikx + kz + \Omega t), \quad \Phi_l = \tilde{\Phi}\exp(ikx - kz + \Omega t)\\ \boldsymbol{\Psi}_l = (0,\ \Psi_l,\ 0), \quad \Psi_l = \Psi\exp(ikx - \tilde{k}z + \Omega t), \quad z^* = Z\exp(ikx + \Omega t)\end{gathered} \tag{9.2}$$

Here Ω is the growth-rate (the characteristic frequency, the eigenvalue) of the system equations (8), $k = 2\pi/\lambda$ is the wavevector and λ is the spatial period (the wavelength).

For the pressure perturbations $p_{h(l)}$ and for the length-scale of the vortical field $\tilde{\lambda} = 2\pi/\tilde{k}$, we obtain from equation (8.2)

$$\nabla\left(\dot{\Phi}_{h(l)} + V_{h(l)}\left(\frac{\partial\Phi_{h(l)}}{\partial z}\right) + \frac{p_{h(l)}}{\rho_{h(l)}}\right) = 0, \quad \left(\frac{\partial}{\partial t} + V_l\frac{\partial}{\partial z}\right)(\nabla\times\boldsymbol{\Psi}_l) = 0 \tag{9.3}$$

The perturbed pressure is free from contributions from the perturbed vortical field [20, 21]. This leads to

$$p_{h(l)} = -\rho_{h(l)}\left(\dot{\Phi}_{h(l)} + V_{h(l)}\frac{\partial\Phi_{h(l)}}{\partial z}\right), \quad \tilde{k} = \Omega/V_l \tag{9.4.1}$$

The perturbed enthalpy is

$$w_{h(l)} = \frac{p_{h(l)}}{\rho_{h(l)}} = -\left(\dot{\Phi}_{h(l)} + V_{h(l)}\frac{\partial\Phi_{h(l)}}{\partial z}\right) \tag{9.4.2}$$

accounting for the constancy of internal energy in ideal incompressible fluids. We note that the vortical field wave-vector $\tilde{k} = \Omega/V_l$ depends on the growth-rate Ω. The sign of the real part of $\tilde{k}$ is defined by the sign of Ω, with $\mathrm{Re}\,[\tilde{k}] > 0\ (< 0)$ for $\mathrm{Re}\,[\Omega] > 0\ (< 0)$ for the unstable (stable) dynamics, and the imaginary part of $\tilde{k}$ is defined by the imaginary part of Ω, as $\mathrm{Im}[\tilde{k}] = \mathrm{Im}[\Omega]/V_l$. In order to obey the boundary conditions $\mathbf{u}_l|_{z\to+\infty} = 0$, the vortical field should decay away from the interface, $(\tilde{k}/k) > 0$, and the interface dynamics should be unstable, $\mathrm{Re}\,[\Omega(kV_h)] > 0$.

In the presence of the acceleration $\mathbf{g} = (0,\ 0,\ g)$ and the surface tension the pressure and the enthalpy perturbations are modified as [20–23]:

$$\begin{gathered}p_{h(l)} \to p_{h(l)} + \rho_{h(l)}\ g\ z, \quad (p_h - p_l) \to (p_h - p_l) + \sigma\frac{\partial^2 z^*}{\partial x^2}\\ w_{h(l)} \to w_{h(l)} + \ g\ z, \quad (w_h - w_l) \to (w_h - w_l) + \frac{\sigma}{\rho_h}\frac{\partial^2 z^*}{\partial x^2}\end{gathered} \tag{9.5}$$

The perturbed dynamics is incompressible for a broad range of values of the acceleration, $|\ \rho g/kP_0\ | \ll 1$, and the surface tension, $|\sigma k/P_0| \ll 1$ [20–23].

Figure 1 illustrates the flow configuration, with the heavy (light) fluid located in the lower (upper) part of the domain. The acceleration is directed from the heavy to the light fluid and, similarly to Rayleigh-Taylor instability, destabilizes the dynamics. The locations of the heavy and light fluids and the direction of the acceleration along the z axis are chosen to better illustrate the flow fields of the light fluid and to easier compare the flow fields of the conservative dynamics with interfacial mass flux with those of Landau-Darrieus and Rayleigh-Taylor instabilities [20–23, 32–38, 46].

With expressions equation (9), the system of differential equations governing the interface dynamics is reduced to the linear system $\mathrm{M}\mathbf{r} = 0$, where vector $\mathbf{r}$ is $\mathbf{r} = (\Phi_h,\ \Phi_l,\ V_h z^*,\ \Psi_l)^T$, and the matrix M is defined by the boundary conditions at the interface equations (8), (9) [21].

Dimensionless units: For ideal incompressible fluids, the characteristic length-scale $1/k$ and time-scale $1/kV_h$ are defined by the initial conditions, and the characteristic density scale is set by the heavy fluid density ρ_h. We use the dimensionless values of the growth-rate $\omega = \Omega/kV_h$, and the density ratio $R = \rho_h/\rho_l$ with $R \geqslant 1$. This leads to $V_l/V_h = R, \quad \tilde{k}/k = \omega/R$ [21–23]. We use the dimensionless values of the gravity $G = g/kV_h^2$, with $G \geqslant 0$, and surface tension $T = (\sigma/\rho_h)(k/V_h^2)$, with $T \geqslant 0$, and with a broad range of values $G \geqslant 0$ and $T \geqslant 0$ for incompressible dynamics [20–22]. We use dimensionless values for the flow fields, the interface, and the variables as $\varphi = \Phi/(V_h/k)$, $\tilde{\varphi} = \tilde{\Phi}/(V_h/k)$, $\psi = \Psi/(V_h/k)$, $\bar{z} = kZ$, and $kx \to x$, $kz \to z$, $kV_h t \to t$. In the dimensionless units, the fluid potentials are $\varphi_h = \varphi e^{ix+z+\omega\ t}, \quad \varphi_l = \tilde{\varphi} e^{ix-z+\omega\ t}$ and $\boldsymbol{\psi}_l = (0,\ \psi_l,\ 0)$ with $\psi_l = \psi e^{ix-(\tilde{k}/k)z+\omega\ t}$, the fluid velocities are $\mathbf{u}_h = \nabla\varphi_h, \quad \mathbf{u}_l = \nabla\varphi_l + \nabla \times \boldsymbol{\psi}_l$, and the interface perturbation is $z^* = \bar{z} e^{ix+\omega\ t}$.

Fundamental solutions: In the dimensionless form, the elements of the matrix M is are the functions of the growth-rate (the frequency, the eigenvalue) ω, the density ratio R, the acceleration value G, and the surface tension value T as $M = M(\omega,\ R,\ G,\ T)$ [21]. The condition $\det M(\omega_i,\ R,\ G,\ T) = 0$ defines the eigenvalues ω_i and the associated eigenvectors $\tilde{\mathbf{e}}_i$ [21, 22]. The matrix M is 4×4. For a non-degenerate 4×4 matrix, there are 4 fundamental solutions $\mathbf{r}_i = \mathbf{r}_i(\omega_i,\ \tilde{\mathbf{e}}_i)$, $i = 1...4$, with 4 associated eigenvalues ω_i and eigenvectors $\tilde{\mathbf{e}}_i$, corresponding to 4 degrees of freedom and 4 independent variables obeying 4 equations, equations (8), (9).

Solution $\mathbf{r}$ for the system $M\mathbf{r} = 0$ is a linear combination of the fundamental solutions $\mathbf{r}_i$

$$\mathbf{r} = \sum_{i=1}^{4} C_i \mathbf{r}_i \tag{10}$$

Here C_i are the integration constants, and $\mathbf{r}_i = \mathbf{r}_i(\omega_i,\ \tilde{\mathbf{e}}_i)$ are the fundamental solutions with $\mathbf{r}_i = \tilde{\mathbf{e}}_i e^{\omega_i t}$ and $\tilde{\mathbf{e}}_i = (\varphi e^{ix+z},\quad \tilde{\varphi} e^{ix-z},\quad \bar{z} e^{ix},\quad \psi e^{ix-(\tilde{k}/k)\ z})_{\mathrm{i}}^{\mathrm{T}}$ and with the associated vector $\mathbf{e}_i = (\varphi,\quad \tilde{\varphi},\quad \bar{z},\quad \psi)_{\mathrm{i}}^{\mathrm{T}}$.

At the first glance, the material in section 2 - Method may appear rather formal. This detailed consideration is however necessary, because it related the physics of the interface dynamics to the mathematical attributes of rigorous solutions [21–23, 46]. By using the general matrix method for solving the boundary value problem equations (1)–(10), we directly link the microscopic interfacial transport to the macroscopic flow fields, conduct a systematic study of the interplay of the interface stability with the structure of the flow fields, and investigate the properties of the interface dynamics in a broad parameter regime [21, 22].

2.4. Theory outline

In this work we develop the general framework for theoretical studies of the interface dynamics in a broad range of conditions. Our approach has a number of methodical advantages. (1) Interfacial boundary conditions, which we use, are exact, since they are derived from the conservation laws and in the inertial frame of reference in equations (1), (2). This derivation is free from the postulate of constancy of the interface velocity; it allows us to identify the macroscopic stabilization mechanism and to examine sensitivity of the interface dynamics to the boundary conditions [21–23, 46]. (2) Flow fields, which we employ, are represented by scalar and vector potentials equation (9). This representation permits us to find the structure of the flow fields, to directly link the macroscopic flow quantities far from interface to microscopic transports at the interface, and to quantify dependence of scalar and vector fields on physical parameters of the flow [21–23, 46]. (3) Solutions, which we obtain, are mathematically rigorous and physically complete. This rigorous approach enables us to investigate the degeneracy of non-equilibrium dynamics, to evaluate its sensitivity to initial conditions, and to predict the existence of scale-dependent and self-similar regimes [21–23, 46].

In this work, we consider the dynamics of the fluids and the interface in the inertial frame of reference, when the acceleration is due to the body force and is directed from the heavy to the light fluid equations (1)–(10). This formulation permits the studies of the interface dynamics with the interfacial mass flux (as in conservative dynamics and in Landau-Darrieus instability) and with zero interfacial mass (as in Rayleigh-Taylor instability) in a unified theoretical framework. It also allows the identification of the inertial stabilization mechanism (to be discussed in the next sections), as well as enables the investigations of the linear and nonlinear dynamics.

The interface dynamics is a corner-stone problem of applied mathematics and theoretical physics; it seeded the development of methods of nonlinear analysis and the field of dynamical systems [20, 34, 54]. For the weakly nonlinear dynamics, it inspired the formulation of generic mathematical models, including Ginzburg-Landau, nonlinear Schrödinger, and Kuramoto-Sivashinsky equations [20, 34, 54]. For the highly nonlinear dynamics, it enabled the development of group theory based approach [19, 28, 29]. For self-similar mixing, it provided grounds for development of theory of turbulence, mixing and chaos [19, 20, 29, 34, 54]. Our present work is focused on the linear dynamics and is applicable for small amplitudes and early times, with $t < \Omega^{-1}$ in dimensional units. Our approach can be extended to analyze the weakly nonlinear dynamics at $t \sim \Omega^{-1}$ and late-time nonlinear dynamics at $t \gg \Omega^{-1}$. It can be linked to traditional weakly-nonlinear and highly nonlinear theories [19, 20, 28–31, 34, 54]. We address these important studies to the future.

3. Results

3.1. Matrixes and fundamental solutions

In this section we identify the fundamental solutions for the accelerated conservative dynamics and for the classical Landau's and Rayleigh-Taylor dynamics with the acceleration and surface tension.

3.1.1. Conservative dynamics

We consider the conservative dynamics balancing the fluxes of mass, momentum and energy at the interface, equation (8.1). For this dynamics, the matrix M is $M = M_{GT}$:

$$\mathrm{M}_{GT} = \begin{pmatrix} -R & -1 & -\omega + R\omega & i \\ 1 & -1 & 1 - R & i\omega/R \\ R - R\omega & R + \omega & G(R-1) - RT & -2iR \\ \omega & -\omega & T + \omega - R\omega & iR \end{pmatrix} \tag{11.1}$$

Its determinant is
$\det\ \mathrm{M}_{GT} = i((R-1)/R)(\omega - R)(\omega + R)(\omega^2(R-1) + R(R-1) - G(R+1) + TR)$, and the values ω_i and $\mathbf{e}_i$ are

$$\omega_{1(2)} = \pm i\sqrt{R}\sqrt{1 - \frac{G(R+1)}{R(R-1)} + \frac{T}{R-1}}, \quad \mathbf{e}_{1(2)} = (\varphi, \ \tilde{\varphi}, \ 1, \ \psi)^{\mathrm{T}}_{1(2)};$$
$$\omega_3 = R, \quad \mathbf{e}_3 = (0, \ i, \ 0, \ 1)^T; \quad \omega_4 = -R, \quad \mathbf{e}_4 = \left(\frac{2i}{R+1}, \ -\frac{i(R-1)}{R+1}, \ 0, \ 1\right)^{\mathrm{T}} \tag{11.2}$$

where the components $\{\varphi, \tilde{\varphi}, \psi\}$ of the eigenvectors for solutions 1 and 2 are functions on R, G, T. Among the fundamental solutions for the conservative dynamics equation (11), the fundamental solutions $\mathbf{r}_1(\omega_1, \mathbf{e}_1)$ and $\mathbf{r}_2(\omega_2, \mathbf{e}_2)$ depend on the values of the acceleration G and the surface tension T, whereas the fundamental solutions $\mathbf{r}_3(\omega_3, \mathbf{e}_3)$ and $\mathbf{r}_4(\omega_4, \mathbf{e}_4)$ are independent of G and T [21, 22].

In regards to the fundamental solutions $\mathbf{r}_1(\omega_1, \mathbf{e}_1)$ and $\mathbf{r}_2(\omega_2, \mathbf{e}_2)$ in equation (11), for some values of the acceleration, the surface tension and the density ratio, these solutions are stable, with $\mathbf{r}_1 = \mathbf{r}_2^*$ and $\omega_1 = \omega_2^*$ with $\mathrm{Re}\,[\omega_{1(2)}] = 0$. They describe two stable traveling waves, whose superposition results in stably oscillating standing waves. For some other values of the acceleration, the surface tension and the density ratio, one of these solutions is unstable, $\mathbf{r}_1$ with $\mathrm{Re}[\omega_1] > 0$, whereas the other is stable, $\mathbf{r}_2$ with $\mathrm{Re}\,[\omega_2] > 0$. These solutions describe the standing waves, with the growing ($\mathbf{r}_1$) and the decaying ($\mathbf{r}_2$) amplitudes. For these solutions, the interface perturbations are coupled with the potential and vortical components of the velocities of the fluids' bulk.

In regards to the fundamental solutions $\mathbf{r}_3(\omega_3, \mathbf{e}_3)$ and $\mathbf{r}_4(\omega_4, \mathbf{e}_4)$ in equation (11), the solution $\mathbf{r}_3$ is unstable, $\omega_3 = R$ and $\mathrm{Re}\,[\omega_3] > 0$, and the solution $\mathbf{r}_4$ is stable, $\omega_4 = -R$ and $\mathrm{Re}\,[\omega_4] < 0$. The remarkable property of the formally unstable solution $\mathbf{r}_3$ is that the interface perturbation and the perturbed fields of the velocities and pressure are identically zero in the entire domain at any time for any integration constant C_3, with $z^* = 0, \quad \mathbf{u}_{h(l)} = 0, \quad p_{h(l)} = 0$ [21, 22]. For the formally stable fundamental solution $\mathbf{r}_4$, we must set the integration constant $C_4 = 0$, in order for this solution to obey at any time the conditions $\mathbf{u}_l|_{z\to+\infty} = 0$. This is because the vortical component of the velocity, $\nabla \times \boldsymbol{\psi}_l \neq 0$, while decaying in time, increases away from the interface. Note that for solution $\mathbf{r}_4$ the vorticity value is $\nabla \times \mathbf{u}_l = 0$, despite of $\boldsymbol{\psi}_l \neq 0$ and $\nabla \times \boldsymbol{\psi}_l \neq 0$. This is because in the vorticity field $\nabla \times \mathbf{r}_l = (0, \ (1 - (\tilde{k}/k)^2) \ \psi_l, \ 0)$ the values are $(\tilde{k}/k)^2 = (\omega/R)^2 = 1$ [21, 22].

The accelerated conservative dynamics with surface tension has 4 fundamental solutions with 4 associated eigenvalues and eigenvectors, 4 independent degrees of freedom, and is non-degenerate. By defining the solution $\mathbf{r}_{CDGT}$ in the stable regime as the superposition of the traveling waves $\mathbf{r}_{CDGT} = (\mathbf{r}_1 + \mathbf{r}_2)/2$ and in the unstable regime as the solution $\mathbf{r}_{CDGT} = \mathbf{r}_1$, we analyze properties of this solution below, table 1. Sub-script stands for conservative dynamics with the gravity G and the surface tension T.

3.1.2. Classical Landau's dynamics

The Landau's theory for Landau-Darrieus instability, hereafter - the classical Landau's dynamics, balances the fluxes of mass, and normal and tangential components of momentum, and employs the special condition for the perturbed velocity at the interface. This special condition postulates the constancy of the interface velocity of the non-steady non-planar interface, $\tilde{\mathbf{V}} \equiv \tilde{\mathbf{V}}_0$, and leads to [20–23, 32–35, 46]:

Table 1. Fundamental solution for the conservative dynamics with the acceleration and the surface tension.

$\mathbf{r} = \mathbf{r}_{CDGT}, \omega = \omega_{CDGT}, \mathbf{e} = \mathbf{e}_{CDGT} = (\varphi, \tilde{\varphi}, \bar{z}, \psi)^T_{CDGT}$	
ω	$\frac{\sqrt{G+R+GR-R^2-RT}}{\sqrt{-1+R}}$
φ	$-\frac{1}{R+G(1+R)-R(R^2+T)}(\sqrt{-1+R}(T\sqrt{R+G(1+R)-R(R+T)}-G(\sqrt{-1+R}+\sqrt{R+G(1+R)-R(R+T)})$ $-R(\sqrt{-1+R}+\sqrt{R+G(1+R)-R(R+T)})+R^2(\sqrt{-1+R}+\sqrt{R+G(1+R)-R(R+T)})))$
$\tilde{\varphi}$	$\frac{1}{-G(1+R)+R(-1+R^2+T)}(G(-1+R)R-G\sqrt{-1+R}\sqrt{R+G(1+R)-R(R+T)}$ $-(-1+R)R((-1+R)R+T-\sqrt{-1+R}\sqrt{R+G(1+R)-R(R+T)})$
$\bar{z}$	1
ψ	$-\frac{\mathrm{i}(-1+R)RT}{R+G(1+R)-R(R^2+T)}$

$$[\mathbf{j}\cdot\mathbf{n}_0]=0,\quad \left[\left(\left(p+\frac{2(\mathbf{J}\cdot\mathbf{n}_0)}{\rho}\right)(\mathbf{j}\cdot\mathbf{n}_0)\right)\mathbf{n}_0\right]=0,$$
$$\left[(\mathbf{J}\cdot\mathbf{n}_0)\frac{(\mathbf{J}\cdot\boldsymbol{\tau}_1+\mathbf{j}\cdot\boldsymbol{\tau}_0)}{\rho}\boldsymbol{\tau}_0\right]=0,\quad [\mathbf{u}\cdot\mathbf{n}_0]=0 \tag{12.1}$$

For the Landau's dynamics the matrix M is $\mathrm{M}=\mathrm{L}_{GT}$.

$$\mathrm{L}_{GT}=\begin{pmatrix} -R & -1 & -\omega+R\omega & i \\ 1 & -1 & 1-R & i\omega/R \\ R-R\omega & R+\omega & G(R-1)-RT & -2iR \\ -1 & -1 & 0 & i \end{pmatrix} \tag{12.2}$$

Its determinant is $\det\ \mathrm{L}_{GT}=i((R-1)/R)(\omega-R)((R+1)\omega^2+2R\omega-(R-1)(R+G)+TR)$, and the values of ω_i and $\mathbf{e}_i$ are:

$$\omega_{1(2)}=\frac{-R\pm\sqrt{(R^3+R^2-R)+G(R^2-1)-TR(R+1)}}{R+1},\quad \mathbf{e}_{1(2)}=(\varphi,\ \tilde{\varphi},\ 1,\ \psi)^T_{1(2)};$$
$$\omega_3=R,\quad \mathbf{e}_3=(0,\ i,\ 0,\ 1)^T \tag{12.3}$$

where the components of eigenvectors $\{\varphi,\ \tilde{\varphi},\ \psi\}$ for solutions 1 and 2 are functions on R, G, T.

Among the fundamental solutions for the classical Landau's dynamics, the fundamental solutions $\mathbf{r}_1(\omega_1,\ \mathbf{e}_1)$ and $\mathbf{r}_2(\omega_2,\ \mathbf{e}_2)$ depend on the values of the acceleration G and surface tension T, and the fundamental solution $\mathbf{r}_3(\omega_3,\ \mathbf{e}_3)$ is independent of G and T and is identical to that in equation (11) [21, 22].

For the classical Landau's dynamics equation (12), the fundamental solution $\mathbf{r}_1(\omega_1,\ \mathbf{e}_1)$ corresponds to Landau-Darrieus instability in the gravity field in the presence of the surface tension. For this solution, the interface perturbations are coupled with the potential and vortical components of the velocities in the fluids' bulk. For the fundamental solution $\mathbf{r}_2(\omega_2,\ \mathbf{e}_2)$ the interface perturbation and the potential and vortical components of the velocities are also coupled. For this solution we must set the integration constant $C_2=0$, in order to obey at any time the condition $\mathbf{u}_l|_{z\to+\infty}=0$ in equation (8). Solution $\mathbf{r}_3(\omega_3,\ \mathbf{e}_3)$ has zero fields of the perturbed velocity and pressure in the entire domain for any integration constant C_3 and at any time, as in equation (12) [21, 22].

The accelerated Landau's dynamics with the surface tension is degenerate, since it has smaller number of fundamental solutions (3) than the number of the degrees of freedom (4). This indicates a singular and ill-posed character of the dynamics. The lifting the degeneracy may lead to a scale-invariant power-law dynamics and be triggered by a seed vortical field, pre-imposed in the bulk of the light fluid at some instance of time [21].

By defining the solution as $\mathbf{r}_{LDGT}=\mathbf{r}_1$, we analyze properties of this solution below, table 2. Sub-script stands for Landau's dynamics with the gravity and the tension.

3.1.3. Rayleigh-Taylor dynamics

In theory of Rayleigh-Taylor instability - Rayleigh-Taylor dynamics hereafter - another set of the interfacial boundary conditions is employed in order to describe the interface with zero interfacial mass flux, which may also be called a contact discontinuity and an interface between immiscible fluids [20–31]. For outline of theoretical, numerical and experimental works on RTI, the reader is referred to edited research book and to review and research papers [2, 7, 18, 19, 24–31, 41, 52, 53, 55, 56, 57–60] and references therein.

The boundary conditions equations (2)–(4) are derived from the governing equations equation (1) assuming that the mass flux is conserved at the interface, $[\tilde{\mathbf{j}}\cdot\mathbf{n}]=0$. There is the important particular case, when the conserved mass flux is zero at the interface, $\tilde{\mathbf{j}}\cdot\mathbf{n}|_{\theta=0}=0$. This leads to the continuity of normal component of

Table 2. Fundamental solution for the Landau's dynamics with the acceleration and the surface tension.

$\mathbf{r}=\mathbf{r}_{LDGT}$, $\omega=\omega_{LDGT}$, $\mathbf{e}=\mathbf{e}_{LDGT}=(\varphi,\ \tilde{\varphi},\ \bar{z},\ \psi)^T_{LDGT}$	
ω	$\frac{-R+\sqrt{-G-R+R^2+GR^2+R^3-RT-R^2T}}{1+R}$
φ	$-\frac{R-\sqrt{G(-1+R^2)+R(-1+R+R^2-(1+R)T)}}{1+R}$
$\tilde{\varphi}$	$\frac{1}{(1+R)(R(2+R)-\sqrt{G(-1+R^2)+R(-1+R+R^2-(1+R)T)})}$ $(G-GR^2+R(T+\sqrt{G(-1+R^2)+R(-1+R+R^2-(1+R)T)}$ $+R(-2+R+R^2+T-\sqrt{G(-1+R^2)+R(-1+R+R^2-(1+R)T)}))$
$\bar{z}$	1
ψ	$\frac{iR(-1+R(2+R)-2\sqrt{G(-1+R^2)+R(-1+R+R^2-(1+R)T)})}{R(2+R)-\sqrt{G(-1+R^2)+R(-1+R+R^2-(1+R)T)}}$

velocity $[\mathbf{v}\cdot\mathbf{n}]=0$, the continuity of the pressure, and the arbitrariness of the jumps of tangential component of velocity and enthalpy at the interface [19–22, 28, 29]:

$$[\mathbf{v}\cdot\mathbf{n}]=0,\quad [P]=0,\quad [\mathbf{v}\cdot\boldsymbol{\tau}]=arbitrary,\quad [W]=arbitrary \tag{13.1}$$

For the zero mass flux at the interface, the outside boundaries have no influence on the dynamics:

$$\mathbf{v}|_{z\to+\infty}=0,\quad \mathbf{v}|_{z\to-\infty}=0 \tag{13.2}$$

and the interface velocity is zero in the laboratory frame of reference:

$$\tilde{\mathbf{V}}=0 \tag{13.3}$$

This case corresponds to the dynamics of a contact discontinuity and an interface with between immiscible fluids, and to Rayleigh-Taylor and Richtmyer-Meshkov instabilities. According to the boundary conditions equation (13), in Rayleigh-Taylor dynamics, due to zero mass flux at the interface, the tangential component of velocity is discontinuous at the interface, and the velocity field has the interfacial shear [20–23, 46].

For Rayleigh-Taylor dynamics, the unperturbed interface is planar, and the unperturbed velocity field is zero in both fluids. We slightly perturb the interface as $\theta=-z+z^*(x,\ t)$, with $z^*=Ze^{ikx+\Omega t}$, $|\dot{\theta}/|\nabla\theta||\ll\sqrt{g/k}$ and $|\partial z^*/\partial x|\ll 1$. We slightly perturb the fluid velocities with the potential fields, $\mathbf{v}_h=\nabla\Phi_h$, $\Phi_h=\Phi e^{ikx+kz+\Omega t}$, and $\mathbf{v}_l=\nabla\Phi_l$, $\Phi_l=\tilde{\Phi}e^{ikx-kz+\Omega t}$, with $|\mathbf{v}|\ll\sqrt{g/k}$. We perturb the fluid pressure as $P=P_0+p, |p|\ll|P_0|$, with $p_{h(l)}=-\rho_{h(l)}(\dot{\Phi}_{h(l)}+V_{h(l)}\partial\Phi_{h(l)}/\partial z-gz)$ and further modify it as $(p_h-p_l)\to(p_h-p_l)+\sigma(\partial^2 z^*/\partial x^2)$. System equation (13) is then reduced to a linear system $M\mathbf{r}=0$, where vector $\mathbf{r}$ is $\mathbf{r}=(\Phi_h,\ \Phi_l,\ V_h z^*)^T$ and M is the 3×3 matrix.

In Rayleigh-Taylor dynamics the length-scale is $1/k$ and the time-scale is $1/\sqrt{gk}$. In order to conduct a comparative study of this dynamics with the conservative dynamics and the classical Landau's dynamics, we scale the time with $1/kV_h$, where is now understood as some velocity scale. This leads to $G=g/kV_h^2$ and $T=(\sigma/\rho_h)(k/V_h^2)$, as before. In the dimensional units the matrix $\mathrm{M}=\mathrm{M}(\omega,\ R,\ G,\ T)$. For system $M\mathbf{r}=0$, the solution is $\mathbf{r}=\sum_i C_i\mathbf{r}_i$, with in non-degenerate case, similarly to equation (10). Here C_i are the integration constants, $\mathbf{r}_i=\mathbf{r}_i(\omega_i,\ \tilde{\mathbf{e}}_i)$ are the fundamental solutions with $\mathbf{r}_i=\tilde{\mathbf{e}}_i e^{\omega_i t}$, $\tilde{\mathbf{e}}_i=(\varphi e^{ix+z},\quad \tilde{\varphi}e^{ix-z},\quad \bar{z}e^{ix})_i^{\mathrm{T}}$ are the eigenvectors, and $\mathbf{e}_i=(\varphi_i,\ \tilde{\varphi}_i,\ \bar{z}_i)^T$ are the associated vectors. For Rayleigh-Taylor dynamics in equation (13), matrix M is $\mathrm{M}=\mathrm{T}_{GT}$:

$$\mathrm{T}_{GT}=\begin{pmatrix} -R & -1 & -\omega+R\omega \\ -R-R\omega & -R+\omega & G(R-1)-TR \\ -1 & -1 & 0 \end{pmatrix} \tag{14.1}$$

Its determinant is $det\ \mathrm{T}_{GT}=(R-1)((R+1)\omega^2-G(R-1)+TR)$, and ω_i and $\mathbf{e}_i$ are

$$\omega_{1(2)}=\pm\sqrt{\frac{G(R-1)-TR}{R+1}},\qquad \mathbf{e}_{1(2)}=(\varphi,\quad \tilde{\varphi},\quad 1)^{\mathrm{T}}_{1(2)} \tag{14.2}$$

where the components of eigenvectors $\{\varphi,\quad \tilde{\varphi}\}$ are the functions on $R,\ G,\ T$.

Depending on the values of the acceleration, the surface tension and the density ratio, the solutions $\mathbf{r}_1(\omega_1,\ \mathbf{e}_1)$ and $\mathbf{r}_2(\omega_2,\ \mathbf{e}_2)$ can be stable or unstable. When both solutions are stable, with $\mathbf{r}_1=\mathbf{r}_2^*$ and $\omega_1=\omega_2^*$ with $\mathrm{Re}\,[\omega_{1(2)}]=0$, they describe traveling waves whose superposition results in stably oscillating standing waves. For some other values of the acceleration, the surface tension and the density ratio, one of these solutions is unstable, $\mathbf{r}_1$ with $\mathrm{Re}\,[\omega_1]>0$, whereas the other is stable, $\mathbf{r}_2$ with $\mathrm{Re}\,[\omega_2]>0$. These solutions describe the standing waves, with the growing ($\mathbf{r}_1$) and decaying ($\mathbf{r}_2$) amplitudes. For solutions $\mathbf{r}_1$ and $\mathbf{r}_2$ the velocity fields are potential in the fluids' bulk. For $G>0,\quad R>1,\quad T=0$, solution $\mathbf{r}_1(\omega_1,\ \mathbf{e}_1)$ corresponds to Rayleigh-Taylor instability [19–21, 24–31].

Table 3. Fundamental solution for Rayleigh-Taylor with the acceleration and the surface tension.

$\mathbf{r} = \mathbf{r}_{RTGT}$, $\omega = \omega_{RTGT}$, $\mathbf{e} = \mathbf{e}_{RTGT} = (\varphi, \tilde{\varphi}, \bar{z})^T_{RTGT}$	
ω	$\frac{\sqrt{-1+R}\sqrt{-G+GR-RT}}{\sqrt{-1+R^2}}$
φ	$\frac{\sqrt{-1+R}\sqrt{G(-1+R)-RT}}{\sqrt{-1+R^2}}$
$\tilde{\varphi}$	$-\frac{\sqrt{-1+R}\sqrt{G(-1+R)-RT}}{\sqrt{-1+R^2}}$
$\bar{z}$	1

Rayleigh-Taylor dynamics is degenerate, with smaller number of fundamental solutions (2) than the degrees of freedom (3), and, hence, it is singular and ill-posed. The lifting the degeneracy may lead to a power-law dynamics. Such dynamics can be triggered by a seed vortical field pre-imposed at the interface at some instance of time (e.g., vortex line or the vortex sheet). This happens in, e.g., Richtmyer-Meshkov instability, due to the vorticity deposition at the interface and the impulsive acceleration by the shock [21, 22, 24–31].

By defining the solution as $\mathbf{r}_{RTGT} = (\mathbf{r}_1 + \mathbf{r}_2)/2$ in the stable regime, and as $\mathbf{r}_{RTGT} = \mathbf{r}_1$ in the unstable regime, we analyze properties of this solution below, table 3. Sub-script stands for Rayleigh-Taylor dynamics with the gravity and tension.

3.1.4. Physics properties of mathematical attributes

The important physics outcome of section 3.1 is that in the problem of the interface dynamics the properties of macroscopic flow fields in the bulk are tightly linked to the microscopic transport at the interface. Indeed, for the dynamics conserving the fluxes of mass, momentum and energy at the interface, the fluid velocity may have vortical field in the bulk depending on the values of the acceleration and the surface tension, and is shear-free at the interface. For the classical Landau's dynamics in Landau-Darrieus instability, conserving the fluxes of mass and momentum and having special conditions for the perturbed mass flux at the interface, the fluid velocity field have a vortical field in the bulk, and it is shear-free at the interface. For Rayleigh-Taylor dynamics in Rayleigh-Taylor instability, conserving the fluxes of mass, momentum and energy at the interface and having zero interfacial mass flux, the fluid velocity field is free from vortical field in the bulk, and the velocity field has the interfacial shear. Hence, by diagnosing qualitative macroscopic properties of the flow fields in the bulk away from the interface, one may identify the properties of microscopic transport at the interface. One may deduce, for instance, whether there is an interfacial mass flux, whether the interfacial mass flux is zero, and whether the energy is fully balanced at the interface.

The other important physics outcome of section 3.1 is the identification of a degenerate or a non-degenerate character of the dynamics [20–23, 46]. Our results clearly illustrate that the conservative dynamics is non-degenerate, since it has 4 fundamental solutions for 4 governing equations with 4 independent variables; it is hence complete. The classical Landau's dynamics for Landau-Darrieus instability is degenerate (3 fundamental solutions for 4 governing equations with 4 independent variables). The lifting the degeneracy of Landau-Darrieus instability may lead to scale-invariant (power-law) rather scale-dependent (exponential) dynamics [46]. The Rayleigh-Taylor dynamics for Rayleigh-Taylor instability is also degenerate (2 fundamental solutions for 3 governing equations with 3 independent variables). The lifting the degeneracy of Rayleigh-Taylor unstable dynamics may lead to Richtmyer-Meshkov instability, where a (sub-sonic) initial growth-rate can be set by a shock, and/or an impulsive acceleration. The interested readers are referred to papers [20–29, 46] for details.

3.2. Inertial dynamics free from surface tension

In this sub-section, for the purpose of completeness, we provide solutions $\{\mathbf{r}_{CDGT}, \mathbf{r}_{LDGT}, \mathbf{r}_{RTGT}\}$ for inertial dynamics free from surface tension, $G = 0, \quad T = 0$, see [21] for details.

Conservative dynamics has the solution $\mathbf{r}_{CDGT}|_{G=0,\ T=0} = \mathbf{r}_{CDGT}(\omega_{CDGT}, \tilde{\mathbf{e}}_{CDGT})|_{G=0,T=0}$ with

$$\omega_{CDGT}|_{G=0,\ T=0} = \pm i\sqrt{R}, \quad \mathbf{e}_{CDGT}|_{G=0,\ T=0} = \frac{\mathbf{e}+\mathbf{e}^*}{2}, \quad \mathbf{e} = (\varphi, \quad \tilde{\varphi}, \quad 1, \quad 0)^T$$
$$\tilde{\mathbf{V}} = \tilde{\mathbf{V}}_0 + \tilde{\mathbf{v}}, \quad \tilde{\mathbf{v}}\mathbf{n}_0 = -(\mathbf{u}_h\mathbf{n}_0 + \dot{\theta})|_{\theta=0} \sim e^{\pm i\sqrt{R}t} \tag{15.1}$$

The components of the eigenvector are $\varphi = i(R-1)/(i+\sqrt{R})$ and $\tilde{\varphi} = -(R-1)\sqrt{R}/(i+\sqrt{R})$. This solution is stable. It is stabilized by the inertial mechanism. Mathematically, the mechanism is revealed in stable oscillations of the interface velocity near the constant value $\tilde{\mathbf{V}} = \tilde{\mathbf{V}}_0 + \tilde{\mathbf{v}}$, with $\tilde{\mathbf{v}} \cdot \mathbf{n}_0 \sim e^{\pm i\sqrt{R}t}$. Physically, when the interface is perturbed, the parcels of the heavy fluid and the light fluid follow the interface perturbation thus

causing the change of momentum and energy of the fluid system. Yet, the dynamics is inertial. To conserve the momentum and energy, the interface as whole should slightly change its velocity. This causes the reactive force to occur and stabilize the dynamics [21, 22].

Classical Landau's dynamics has the solution $\mathbf{r}_{LDGT}|_{G=0,\ T=0} = \mathbf{r}_{LDGT}(\omega_{LDGT}, \mathbf{e}_{LDGT})|_{G=0,T=0}$ with

$$\omega_{LDGT}|_{G=0,\ T=0} = \frac{-R + \sqrt{-R + R^2 + R^3}}{1 + R}, \quad \mathbf{e}_{LDGT}|_{G=0,\ T=0} = \mathbf{e}, \quad \mathbf{e} = (\varphi, \ \tilde{\varphi}, \ 1, \ \psi)^{\mathrm{T}}$$
$$\tilde{\mathbf{V}} \equiv \tilde{\mathbf{V}}_0, \quad \tilde{\mathbf{V}} = \tilde{\mathbf{V}}_0 + \tilde{\mathbf{v}}, \quad \tilde{\mathbf{v}}\mathbf{n}_0 = -(\mathbf{u}_h\mathbf{n}_0 + \dot{\theta})|_{\theta=0} \equiv 0 \tag{15.2}$$

The components of the eigenvector $\{\varphi, \ \tilde{\varphi}, \ \psi\}$ are the functions on the density ratio R. This solution is unstable. When the interface is perturbed, the parcels of the heavy fluid and the light fluid follow the interface perturbation thus causing the change of momentum and energy of the fluid system. Yet, the postulated constancy of the interface velocity, $\tilde{\mathbf{V}} \equiv \tilde{\mathbf{V}}_0$, which is implemented in the special boundary condition $[\mathbf{un}_0] \equiv 0$, preempts the occurrence of the reactive force. The interface perturbations grow and Landau-Darrieus instability develops [21, 32].

Rayleigh-Taylor dynamics has the solution $\mathbf{r}_{RTGT}|_{G=0,\ T=0} = \mathbf{r}_{RTGT}(\omega_{RTGT}, \tilde{\mathbf{e}}_{RTGT})|_{G=0,T=0}$ with

$$\omega_{RTGT}|_{G=0,\ T=0} = 0, \quad \mathbf{e}_{CDGT}|_{G=0,\ T=0} = \mathbf{e}, \quad \mathbf{e} = (0, \ 0, \ 1)^T, \quad \tilde{\mathbf{V}} = 0 \tag{15.3}$$

This solution is neutrally stable. It has zero interface velocity in the laboratory frame of reference [21].

Hence, for the inertial dynamics free from surface tension $\{\mathbf{r}_{CDGT}, \ \mathbf{r}_{LDGT}, \ \mathbf{r}_{RTGT}\}_{G=0,\ T=0}$: The conservative dynamics is stable; it has potential flow fields in the fluids' bulk and is shear free at the interface; it is stabilized by the inertial mechanism revealed in stable oscillations of the interface velocity near the constant value. The classical Landau's dynamics is unstable; it has potential and vortical components of the velocity in the fluids' bulk; it is shear free at the interface; it has the postulated constant interface velocity; Rayleigh-Taylor dynamics is neutrally stable; it has zero velocity fields in the fluids' bulk; it has zero interface velocity in the laboratory frame of reference. For detailed discussions of physics properties of the inertial dynamics free from surface tension $\{\mathbf{r}_{CDGT}, \ \mathbf{r}_{LDGT}, \ \mathbf{r}_{RTGT}\}_{G=0,\ T=0}$, the reader is referred to the papers [21–23, 46].

3.3. Inertial dynamics with surface tension

Here we investigate solutions $\{\mathbf{r}_{CDGT}, \ \mathbf{r}_{LDGT}, \ \mathbf{r}_{RTGT}\}$ in the case of the inertial dynamics with the surface tension, $G = 0, \ T > 0$. The results are illustrated by figures 2, 3 and tables 1–4.

3.3.1. Conservative dynamics

For the conservative dynamics the solution is $\mathbf{r}_{CDGT}|_{G=0} = \mathbf{r}_{CDGT}(\omega_{CDGT}, \tilde{\mathbf{e}}_{CDGT})|_{G=0}$ with

$$\omega_{CDGT}|_{G=0} = \pm i\sqrt{R}\sqrt{1 + \frac{T}{R - 1}}, \quad \mathbf{e}_{CDGT}|_{G=0} = \frac{\mathbf{e} + \mathbf{e}^*}{2}, \quad \mathbf{e} = (\varphi, \ \tilde{\varphi}, \ 1, \ \psi)^{\mathrm{T}} \tag{16.1}$$

where quantities $\{\varphi, \ \tilde{\varphi}, \ \psi\}$ are the functions on the density ratio and surface tension $R, \ T$. This solution is consistent with the solution for the inertial conservative dynamics free from surface tension equation (15.1), table 1, with $(\varphi, \ \tilde{\varphi}, \ 1, \ \psi) \to (\varphi, \ \tilde{\varphi}, \ 1, \ 0)$ for $T \to 0$.

The flow field for solution $\mathbf{r}_{CDGT}|_{G=0}$ have the following structure equation (16.1). For the inertial conservative dynamics with finite surface tension value, the velocity field is potential in the heavy fluid bulk, and has potential and vortical components in the light fluid bulk equation (16.1), figure 3, table 1. The appearance of the vortical field in the light fluid bulk is associated with the contribution of surface energy, which defines the strength of the vortical field. In the limit of zero surface tension, the velocity fields are potential in both fluids.

The inertial dynamics with the surface tension $\mathbf{r}_{CDGT}|_{G=0}$ is stable for $R > 1, \ T > \tilde{T}_{cr}|_{G=0}, \tilde{T}_{cr}|_{G=0} = 0$, figure 2, table 4. The eigenvalue $\omega_{CDGT}|_{G=0}$ is imagine, $\mathrm{Re}\,[\omega_{CDGT}|_{G=0}] = 0$. This suggests that the length-scale of the vortical field $\tilde{k} = (k/R)\ \omega_{CDGT}|_{G=0}$ is also imagine, $\mathrm{Re}\,[\tilde{k}] = 0$. Hence, the dynamics $\mathbf{r}_{CDGT}|_{G=0}$ describes the standing wave stably oscillating in time, figure 2. For this wave, in the bulk of the heavy fluid the velocity field is potential; it decays away from the interface. In the bulk of the light fluid, the velocity field has potential and vortical components. Its potential component decays away from the interface. The vortical field is periodic in the x direction with the period $\lambda = 2\pi/k$, and is also periodic in the z direction with the period $\tilde{\lambda} = 2\pi/\tilde{k}$. Hence, this dynamics has the stably oscillating periodic vortical structure with constant amplitude, figure 3. For solution $\mathbf{r}_{CDGT}|_{G=0}$ the vorticity $\nabla \times \mathbf{u}_l = (0, \ (1 - (\tilde{k}/k)^2)\psi_l, \ 0)$ is $\nabla \times \mathbf{u}_l \neq 0$; its field is also periodic in the $(x, \ z)$ plane, figure 3.

Mathematically, the appearance of the vortical and vorticity fields periodic in the z direction of motion is associated with the pure imaginary character of the frequency ω in solution equation (16), which, in turn, defines the purely imaginary wavevector $\tilde{k}$, with $\mathrm{Im}[\tilde{k}] = (k/R)\ \ \mathrm{Im}[\omega_{CDGT}|_{G=0}]$. Physically, by comparing the solutions for the inertial conservative dynamics free from surface tension and with surface tension in

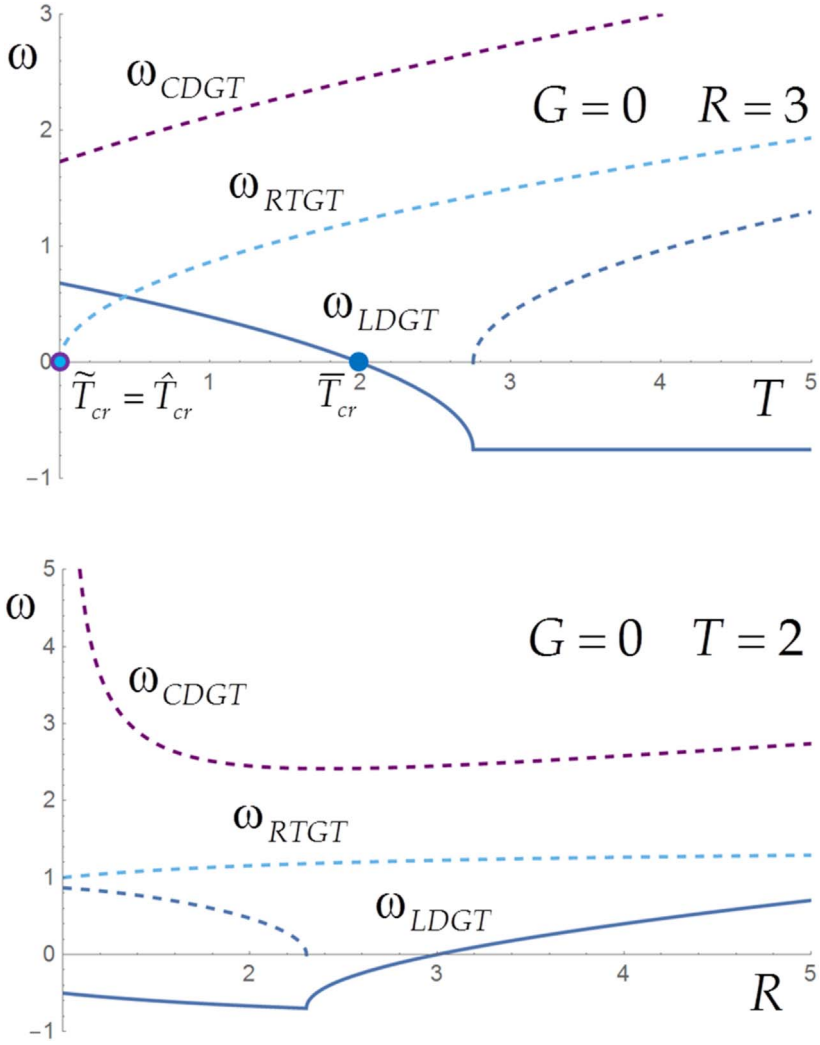

Figure 2. Growth-rates / frequencies for the inertial conservative dynamics (purple), Landau's dynamics (blue) and Rayleigh-Taylor dynamics (light blue) with the surface tension and free from the acceleration. Dependence of the growth-rates: (top) on the surface tension at some value of the density ratio; (bottom) on the density ratio at some value of the surface tension. Solid (dashed) line marks real (imagine) part.

equations (15.1), (16.1), we find that the vortical and vorticity fields are energetic (rather than dynamic) in nature. These fields are decoupled from the pressure field and are produced by the excess of energy, which is caused by the contribution of surface energy to the perturbed enthalpy, equation (9.5), table 1.

Consider now the interplay of the surface tension with the inertial stabilization mechanism. Since the solution is periodic in time, one might expect that the interface velocity experiences stable oscillations, similarly to the case of the inertial dynamics free from surface tension [21]. However, in order to obey the boundary condition $\mathbf{u}_l|_{z\to+\infty} = 0$ in equation (8.2), the solution $\mathbf{r}_{CDGT}|_{G=0}$ in equation (16.1) requires us to set its integration constant equal zero $C_{CDGT}|_{G=0} = 0$. Since the integration constant is zero, the interface velocity for this solution is constant:

$$\tilde{\mathbf{V}} = \tilde{\mathbf{V}}_0 + \tilde{\mathbf{v}}, \quad \tilde{\mathbf{v}}\mathbf{n}_0 = -(\mathbf{u}_h\mathbf{n}_0 + \dot{\theta})|_{\theta=0} \sim e^{\pm i|\omega_{CDGT}|_{G=0}|\,t}, \quad C_{CDGT}|_{G=0} = 0 \Rightarrow \tilde{\mathbf{V}} = \tilde{\mathbf{V}}_0 \tag{16.2}$$

We see that for the conservative dynamics, the inertial stabilization mechanism is present, since the inertial dynamics is stable. This mechanism may however be 'masked' by the surface tension for $T > \tilde{T}_{cr}|_{G=0}$, and may be exhibited at $T = \tilde{T}_{cr}|_{G=0} = 0$.

Note that some slight modifications of the boundary conditions away from the interface $z \to +\infty$ by an external noise may lead to a non-zero integration constant $C_{CDGT}|_{G=0}$ for the dynamics $\mathbf{r}_{CDGT}|_{G=0}$. These modifications may include slight modulations of the uniform velocity field of the light fluid away from the interface, as $\mathbf{V}_l \to \mathbf{V}_l + \delta\mathbf{V}_l$, due to a noisy, which may be present in realistic systems. In this case, the interface velocity for the dynamics $\mathbf{r}_{CDGT}|_{G=0}$ may experience slight oscillations near the constant value, as $\tilde{\mathbf{V}} = \tilde{\mathbf{V}}_0 + \tilde{\mathbf{v}}$ with $\tilde{\mathbf{v}}\mathbf{n}_0 = -(\mathbf{u}_h\mathbf{n}_0 + \dot{\theta})|_{\theta=0} \sim e^{\pm i|\omega_{CDGT}|_{G=0}|\,t}$.

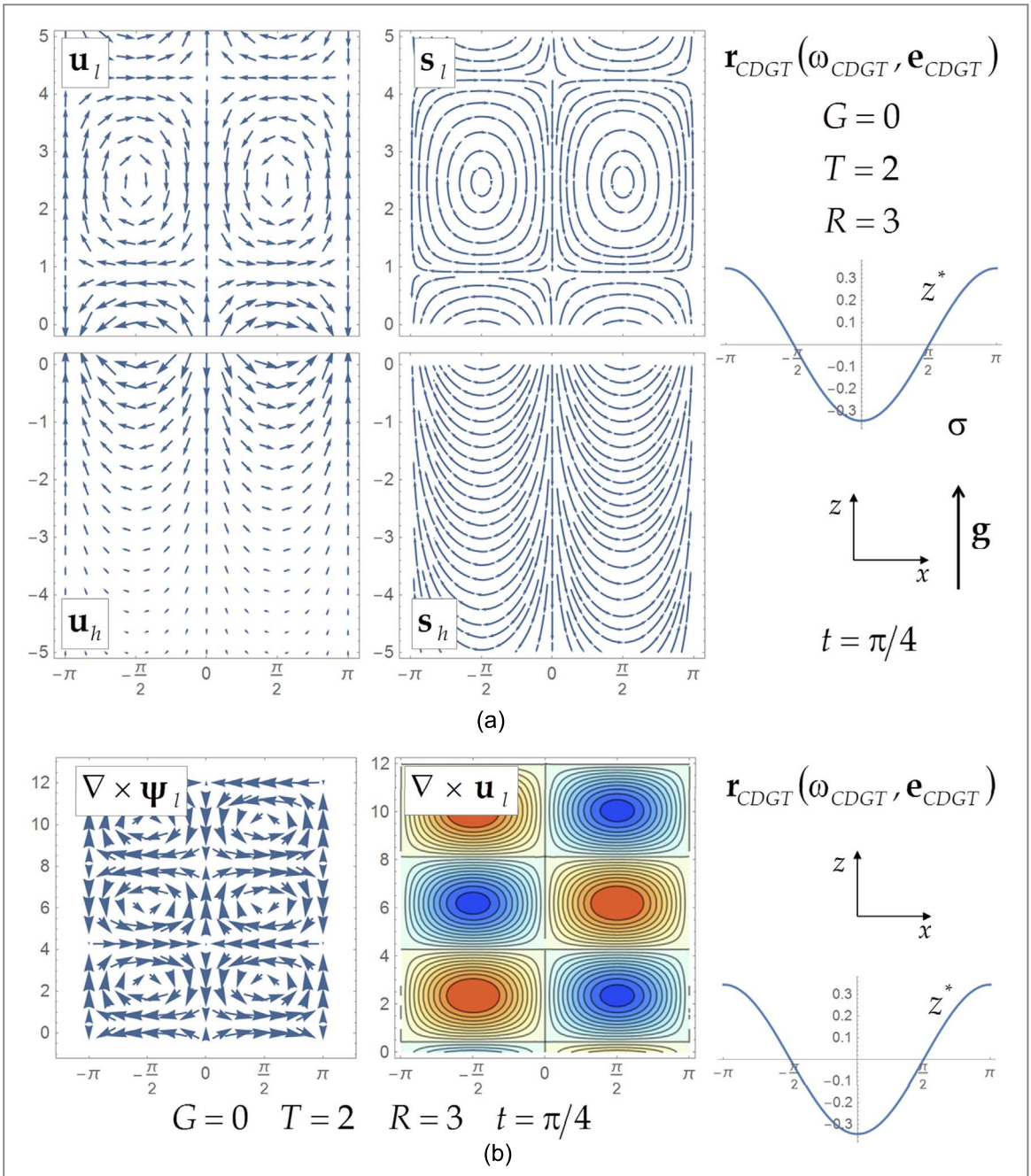

Figure 3. Flow fields for the inertial conservative dynamics with surface tension at some instance of time and at some values of the density ratio and the surface tension: (a) plots of the perturbed velocity vector fields, the perturbed velocity streamlines, and the interface perturbation; (b) plots of the vortical component of the perturbed velocity and the perturbed vorticity. Real parts of fields and functions are shown. Each plot has its own range of values to better present the plot's features.

Table 4. Regions of stability and instability for the inertial acceleration-free dynamics with the surface tension for the conservative, Landau's and Rayleigh-Taylor dynamics.

Dynamics	Stability region	Instability region	Critical value
$\mathbf{r}_{CDGT}\|_{G=0}$	$T > \tilde{T}_{cr}\|_{G=0}$	N/A	$\tilde{T}_{cr}\|_{G=0} = 0$
$\mathbf{r}_{LDGT}\|_{G=0}$	$T > \bar{T}_{cr}\|_{G=0}$	$T < \bar{T}_{cr}\|_{G=0}$	$\bar{T}_{cr}\|_{G=0} = (R-1)$
$\mathbf{r}_{RTGT}\|_{G=0}$	$T > \hat{T}_{cr}\|_{G=0}$	N/A	$\hat{T}_{cr}\|_{G=0} = 0$

Therefore, the inertial conservative dynamics with the surface tension is stable for any values of the density ratio and the surface tension $R > 1, \quad T > \tilde{T}_{cr}|_{G=0}, \tilde{T}_{cr}|_{G=0} = 0$, figures 2, 3, tables 1, 4. The resultant inertial conservative dynamics of the interface with surface tension may correspond to the stable unperturbed flow

fields $(\rho,\ \mathbf{V},\ P_0,\ W_0)_{h(l)}$ and has constant interface velocity $\tilde{\mathbf{V}} = \tilde{\mathbf{V}}_0$ (for zero integration constant $C_{CDGT}|_{G=0} = 0$ of solution $\mathbf{r}_{CDGT}|_{G=0}$). It may also exhibit slightly oscillations of the interface and the interface velocity, as well as the velocity and vorticity fields in the bulk (for non-zero integration constant $C_{CDGT}|_{G=0} = 0$ of solution $\mathbf{r}_{CDGT}|_{G=0}$).

3.3.2. Classical Landau's dynamics

For the classical Landau's dynamics the solution is $\mathbf{r}_{LDGT}|_{G=0} = \mathbf{r}_{LDGT}(\omega_{LDGT},\ \tilde{\mathbf{e}}_{LDGT})|_{G=0}$ with

$$\omega_{LDGT}|_{G=0} = \frac{-R + \sqrt{(R^3 + R^2 - R) - TR(R+1)}}{R+1}, \quad \mathbf{e}_{LDGT}|_{G=0} = \mathbf{e} = (\varphi,\ \tilde{\varphi},\ 1,\ \psi)^{\mathrm{T}} \tag{17}$$

where the quantities $\{\varphi,\ \tilde{\varphi},\ \psi\}$ are the functions on the density ratio and the surface tension $R,\ T$, table 2. This solution is consistent with the solution for classical Landau's dynamics free from surface tension, since for $T \to 0$ components $\{\varphi,\ \tilde{\varphi},\ \psi\}_{LDGT|_{G=0}} \to \{\varphi,\ \tilde{\varphi},\ \psi\}_{LDGT|_{G=0,\ T=0}}$ in agreement with equation (15.2).

The solution $\mathbf{r}_{LDGT}|_{G=0}$ is stable for $T > \bar{T}_{cr}|_{G=0}$, and is unstable for $T < \bar{T}_{cr}|_{G=0}$, where $\bar{T}_{cr}|_{G=0} = R - 1$, in agreement with [20, 21], figure 2, table 4.

The investigation of properties of the solution $\mathbf{r}_{LDGT}|_{G=0}$ for $T > \bar{T}_{cr}|_{G=0}$ suggests that in the stable regime, its integration constant must be set zero $C_{LDGT}|_{G=0} = 0$ in order to obey the boundary conditions far from the interface.

Consider properties of the solution $\mathbf{r}_{LDGT}|_{G=0}$ in the unstable regime, for $T < \bar{T}_{cr}|_{G=0}$, figure 2, table 4. This solution corresponds to Landau-Darrieus instability with surface tension, and satisfies the assigned boundary conditions at the interface and at the outside boundaries of the domain equation (12). Its dynamics couples the interface perturbation with the vortical and potential components of the velocity fields. For solution $\mathbf{r}_{LDGT}|_{G=0}$ the vortical component of the velocity of the light fluid $\nabla \times \boldsymbol{\psi}_l$ and the vorticity $\nabla \times \mathbf{u}_l$, while increasing in time, decay far from the interface. The vortical field has the wavevector $\tilde{k} = (k/R)\ \omega_{LDGT}|_{G=0}$ and the length-scale $\tilde{\lambda}/\lambda = k/\tilde{k}$, figure 2, table 2. The interface velocity for the solution $\mathbf{r}_{LDGT}|_{G=0}$ is constant, $\tilde{\mathbf{V}} \equiv \tilde{\mathbf{V}}_0$, in both stable and unstable regimes, as postulated by the interfacial boundary conditions in the classical Landau's dynamics, equation (12).

3.3.3. Rayleigh-Taylor dynamics

For the inertial Rayleigh-Taylor dynamics of contact discontinuity with surface tension the solution is $\mathbf{r}_{RTGT}|_{G=0} = \mathbf{r}_{RTGT}(\omega_{RTGT},\ \tilde{\mathbf{e}}_{RTGT})|_{G=0}$:

$$\omega_{RTGT}|_{G=0} = \pm i\sqrt{\frac{T\ R}{R+1}}, \quad \mathbf{e}_{CDGT}|_{G=0} = \frac{\mathbf{e} + \mathbf{e}^*}{2}, \quad \mathbf{e} = (\varphi,\ \tilde{\varphi},\ 1)^T \tag{18}$$

This solution is stable. For $T > \hat{T}_{cr}|_{G=0}, \quad \hat{T}_{cr}|_{G=0} = 0$, the solution corresponds to a standing capillary wave stably oscillating in time. At $T = 0$ the solution is neutrally stable, and the components of this solution are $\{\varphi,\ \tilde{\varphi}\}_{RTGT|_{G=0}} = \{0,\ 0\}_{RTGT|_{G=0,\ T=0}}$, figure 2, tables 3, 4.

3.3.4. Summary of properties

Compare the properties of the solutions $\{\mathbf{r}_{CDGT},\ \mathbf{r}_{LDGT},\ \mathbf{r}_{RTGT}\}_{G=0}$ for inertial dynamics with surface tension, figures 2, 3, tables 1–4.

The conservative dynamics is stable for surface tension values $T > \tilde{T}_{cr}|_{G=0}, \quad \tilde{T}_{cr}|_{G=0} = 0$. The presence of the surface tension may 'masks' the inertial stabilization mechanism. The resultant dynamics $\mathbf{r}_{CDGT}|_{G=0}$ may corresponds to stable unperturbed flow fields with constant interface velocity. In the presence of noise, it may also exhibit stable oscillations of the interface and the interface velocity, as well as the velocity and vorticity fields.

The classical Landau's dynamics for Landau-Darrieus instability is stable for $T > \bar{T}_{cr}|_{G=0}$ and is unstable for $T < \hat{T}_{cr}|_{G=0}$ with $\bar{T}_{cr}|_{G=0} = R - 1$. In the stable regime, the dynamics corresponds to the unperturbed flow fields. In the unstable regime, it couples the interface perturbation to the potential and vortical components of the velocity fields in the bulk and it is shear-free at the interface. The classical Landau's dynamics postulates the constancy of the interface velocity.

The inertial Rayleigh-Taylor dynamics is stable for $T > \hat{T}_{cr}|_{G=0}, \quad \hat{T}_{cr}|_{G=0} = 0$. In the stable regime it describes the stably oscillating capillary wave. The dynamics has potential velocity fields in the bulk and has the interfacial shear. The interface velocity is zero in the laboratory frame of reference.

3.3.5. Physics properties of mathematical attributes

For the inertial dynamics, the interface stability and the structure of the flow fields are defined by the interfacial boundary conditions [21–24, 46]. By diagnosing the macroscopic flow fields far from the interface, one may deduce the properties of the microscopic transport at the interface and differentiate between various dynamics. For instance, the observations of stable oscillations of the interface, the vortex-free velocity fields and the zero interface velocity are indicative of Rayleigh-Taylor dynamics with the vanishing interfacial mass flux. The observation of

unstable growth of the interface for small surface tension values, the large-scale vorticity field and the constant interface velocity are indicative of the classical Landau's dynamics, the Landau-Darrieus instability and the energy imbalance at the interface. The observations of the stably oscillating interface and the stably oscillating interface velocity are indicative of the conservative inertial dynamics in the presence of slight noise. These qualitative and quantitative results can be applied for design and interpretation of experimental and observational data.

3.4. Accelerated dynamics free from surface tension

In this sub-section, for the purpose of completeness, we briefly provide the properties of solutions $\{\mathbf{r}_{CDGT},\ \mathbf{r}_{LDGT},\ \mathbf{r}_{RTGT}\}$ for the accelerated dynamics free from surface tension, $G>0,\quad T=0$ [21, 22]. The details can be found in [21, 22].

Conservative dynamics has the solution $\mathbf{r}_{CDGT}|_{\ T=0}=\mathbf{r}_{CDGT}(\omega_{CDGT},\tilde{\mathbf{e}}_{CDGT})|_{T=0}$ with

$$G<G_{cr},\quad \omega_{CDGT}|_{T=0}=\pm i\sqrt{R}\sqrt{1-\frac{G}{G_{cr}}},\quad \mathbf{e}_{CDGT}|_{\ T=0}=\frac{\mathbf{e}+\mathbf{e}^*}{2},\quad \mathbf{e}=(\varphi,\ \tilde{\varphi},\ 1,\ 0)^T;$$
$$G>G_{cr},\quad \omega_{CDGT}|_{T=0}=\sqrt{R}\sqrt{\frac{G}{G_{cr}}-1},\quad \mathbf{e}_{CDGT}|_{\ T=0}=\mathbf{e}=(\varphi,\ \tilde{\varphi},\ 1,\ 0)^T,\quad G_{cr}=\frac{R(R-1)}{R+1};$$
$$\tilde{\mathbf{V}}=\tilde{\mathbf{V}}_0+\tilde{\mathbf{v}},\quad \tilde{\mathbf{v}}\mathbf{n}_0=-(\mathbf{u}_h\mathbf{n}_0+\dot{\theta})|_{\theta=0}\sim e^{(\omega_{CDGT}|_{\ T=0})\ t} \tag{19.1}$$

where quantities $\{\varphi,\ \tilde{\varphi}\}$ are the functions on the density ratio and the acceleration R, G, and G_{cr} is the critical threshold value of the acceleration. For $G\to 0$, this solution is consistent with the solution for the inertial dynamics free from surface tension equation (15.1). For $G>0$ the solution's stability is defined by the interplay of the buoyancy and the inertia, or the gravity and the reactive force. For small acceleration values, $G<G_{cr}$, the inertial effect dominates, and the reactive force exceeds the gravity. The solution is stable, and describes the standing wave stably oscillating in time. The flow dynamics is similar to the case of the inertial conservative dynamics free from surface tension. For large acceleration values, $G>G_{cr}$, the buoyant effect dominates, and the gravity exceeds the reactive force. The solution is unstable, and describes the standing wave with the growing amplitude. For this solution the velocity field is potential in the bulk, and is shear free at the interface. The flow is the superposition of two motions – the motion of the interface as whole with the growing interface velocity and the growth of the interface perturbations [21, 22].

Classical Landau's dynamics has the solution $\mathbf{r}_{LDGT}|_{\ T=0}=\mathbf{r}_{LDGT}(\omega_{LDGT},\tilde{\mathbf{e}}_{LDGT})|_{T=0}$ with

$$\omega_{LDGT}|_{\ T=0}=\frac{-R\pm\sqrt{(R^3+R^2-R)+G(R^2-1)}}{R+1},\quad \mathbf{e}_{LDGT}|_{\ T=0}=\mathbf{e}=(\varphi,\ \tilde{\varphi},\ 1,\ \psi)^{\mathrm{T}}$$
$$\tilde{\mathbf{V}}=\tilde{\mathbf{V}}_0+\tilde{\mathbf{v}},\quad \tilde{\mathbf{v}}\mathbf{n}_0=-(\mathbf{u}_h\mathbf{n}_0+\dot{\theta})|_{\theta=0}\equiv 0,\quad \tilde{\mathbf{V}}\equiv\tilde{\mathbf{V}}_0 \tag{19.2}$$

where quantities $\{\varphi,\ \tilde{\varphi},\ \psi\}$ are the functions on the density ratio and the acceleration R, G. For $G\to 0$, this solution is consistent with that for the inertial Landau's dynamics free from surface tension equation (15.2). This solution is unstable for $G\geqslant 0$ and describes the standing wave with the growing amplitude. Its velocity field is potential in the bulk of the heavy fluid, has vortical and potential components in the bulk of the light fluid, and is shear free at the interface. The flow is the superposition of two motions – the motion of the interface with the postulated constant velocity and the growth of the interface perturbations [20–22].

Rayleigh-Taylor dynamics has the solution $\mathbf{r}_{RTGT}|_{\ T=0}=\mathbf{r}_{RTGT}(\omega_{RTGT},\tilde{\mathbf{e}}_{RTGT})|_{T=0}$ with

$$\omega_{RTGT}|_{\ T=0}=\sqrt{\frac{G(R-1)}{R+1}},\quad \mathbf{e}_{RTGT}|_{\ T=0}=\mathbf{e}=(\varphi,\ \tilde{\varphi},\ 1)^T,\quad \tilde{\mathbf{V}}\equiv 0 \tag{19.3}$$

where quantities $\{\varphi,\ \tilde{\varphi}\}$ are the functions on the density ratio and the acceleration R, G. This solution is unstable for any $G>0$ and describes the standing wave with the growing amplitude. Its velocity field is potential in the bulks of the heavy and the light fluids, and has shear at the interface. In the laboratory frame of reference the interface velocity is zero [20–22].

A brief comparison of properties of the solutions $\{\mathbf{r}_{CDGT},\ \mathbf{r}_{LDGT},\ \mathbf{r}_{RTGT}\}_{T=0}$ in equation (19) suggests: The accelerated conservative dynamics is unstable when the acceleration magnitude exceeds a threshold value set by inertial stabilization mechanism, $G>G_{cr}$; it has the growing interface velocity in the unstable regime; it has potential flow fields in the fluids' bulk, and is shear free at the interface. The accelerated Landau's dynamic is unstable for the acceleration values $G\geqslant 0$; it has a postulated constant interface velocity preempting the inertial stabilization mechanism to occur; it has a potential velocity field in the heavy fluid bulk and potential and vortical velocity fields in the light fluid bulk; it is shear free at the interface. Rayleigh-Taylor dynamics is unstable for any acceleration value $G>0$; it has zero interface velocity in the laboratory frame of reference; it has potential velocity fields in the fluids' bulk, and it has the interfacial shear. For large acceleration values $G>G^*$, $G^*=(R^2-1)/4$ the instability of the accelerated conservative dynamics has the largest growth-rate

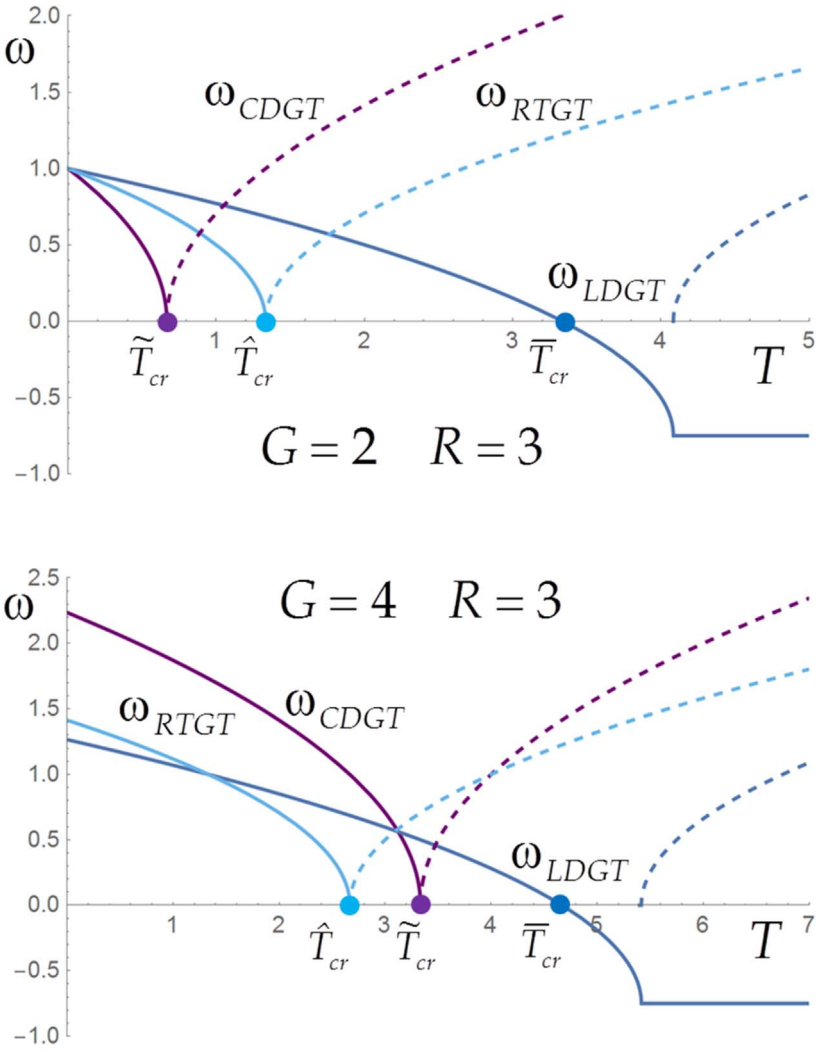

Figure 4. Growth-rates / frequencies for the accelerated conservative dynamics (purple), Landau's dynamics (blue) and Rayleigh-Taylor dynamics (light blue) with the surface tension at some values of the density ratio and the acceleration: Dependence of the growth-rates on the surface tension for (top) weak and (bottom) intermediate accelerations. Solid (dashed) line marks real (imagine) part.

when compared to the cases of the Landau-Darrieus and Rayleigh-Taylor instabilities, see for details [20–30]. The reader is referred to the papers [21–23, 46] for detailed discussions of physics properties of the accelerated dynamics free from surface tension $\{\mathbf{r}_{CDGT},\ \mathbf{r}_{LDGT},\ \mathbf{r}_{RTGT}\}_{T=0}$,.

3.5. Accelerated dynamics with surface tension

In this section we investigate the properties of the solutions $\{\mathbf{r}_{CDGT},\ \mathbf{r}_{LDGT},\ \mathbf{r}_{RTGT}\}$ for the accelerated dynamics with surface tension, $G > 0,\quad T > 0$, figures 4–9, tables 1–3, 5, 6.

3.5.1. Conservative dynamics

Fundamental solution: For the accelerated conservative dynamics with the surface tension the solution is $\mathbf{r}_{CDGT} = \mathbf{r}_{CDGT}(\omega_{CDGT}, \tilde{\mathbf{e}}_{CDGT})$, figures 4–7, tables 1, 5:

$$\tilde{G} < G_{cr},\quad \omega_{CDGT} = \pm i\sqrt{R}\sqrt{1-\frac{\tilde{G}}{G_{cr}}},\quad \mathbf{e}_{CDGT} = \frac{\mathbf{e}+\mathbf{e}^*}{2},\quad \mathbf{e} = (\varphi,\ \tilde{\varphi},\ 1,\ \psi)^{\mathrm{T}};$$

$$\tilde{G} > G_{cr},\quad \omega_{CDGT} = \sqrt{R}\sqrt{\frac{\tilde{G}}{G_{cr}}-1},\quad \mathbf{e}_{CDGT} = \mathbf{e} = (\varphi,\ \tilde{\varphi},\ 1,\ \psi)^{\mathrm{T}};$$

$$\tilde{G} = G - \frac{T\ R}{R+1},\quad G_{cr} = \frac{R(R-1)}{R+1};$$

$$\tilde{\mathbf{V}} = \tilde{\mathbf{V}}_0 + \tilde{\mathbf{v}},\quad \tilde{\mathbf{v}}\mathbf{n}_0 = -(\mathbf{u}_h\mathbf{n}_0 + \dot{\theta})|_{\theta=0} \sim e^{|\omega_{CDGT}|_{T=0}|\,t} \tag{20}$$

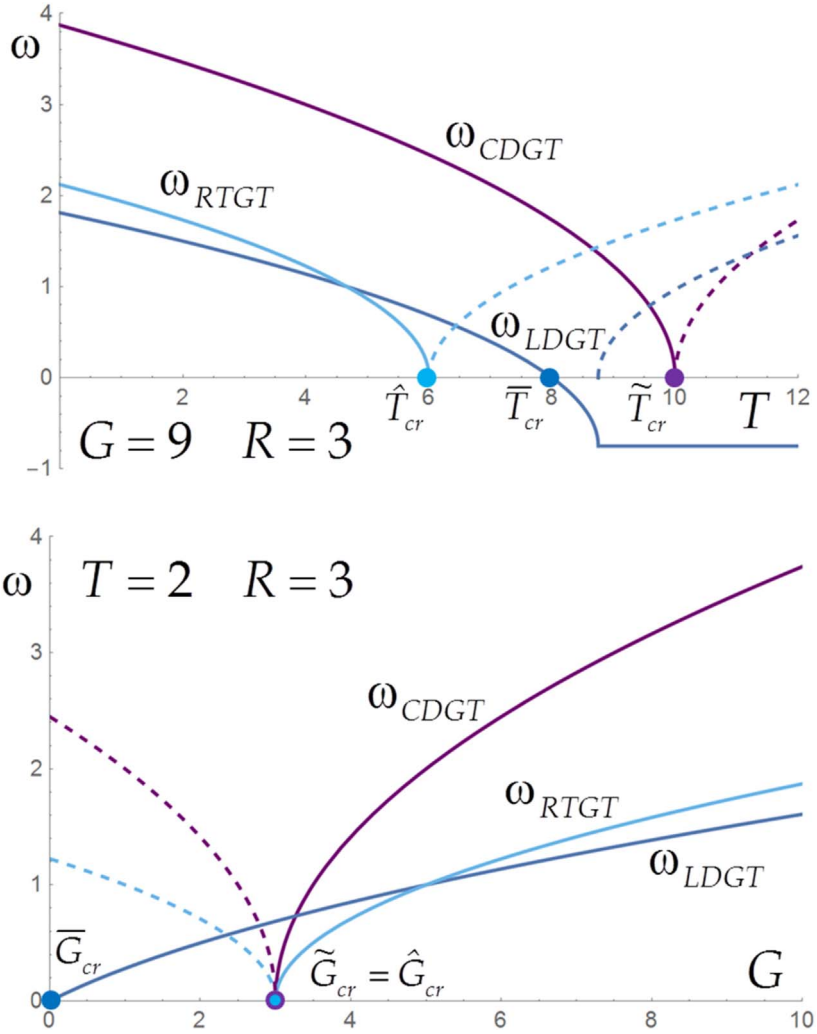

Figure 5. Growth-rates / frequencies for the accelerated conservative dynamics (purple), Landau's dynamics (blue) and Rayleigh-Taylor dynamics (light blue) with the surface tension at some value of the density ratio. Dependence of the growth-rates: (top) on the surface tension at some acceleration value for strong accelerations; (bottom) on the acceleration at some values of the surface tension. Solid (dashed) line marks real (imagine) part.

where the modified acceleration $\tilde{G}$ accounts the contribution of the surface tension T, and G_{cr} is the critical threshold acceleration value in the zero surface tension case. The quantities $\{\varphi,\ \tilde{\varphi},\ \psi\}$ depend on the density ratio, the acceleration and the surface tension $R,\ G,\ T$. The vortical field is $\psi = -iT\ R(R-1)/(G(R+1) - R(R^2+T-1))$, with $\psi|_{T=0} = 0$. This solution is consistent with the solution equation (19.1) for the accelerated conservative dynamics free from surface tension.

Stability and instability of the fundamental solution: For $G > 0$ the stability of the solution $\mathbf{r}_{CDGT}$ is defined by the interplay of the buoyancy, the inertia and the surface tension, or - the gravity, the reactive force and the tension force. The stability curve is defined by the condition $\tilde{G} = G_{cr}$ balancing the buoyancy (the gravity) with the combined contributions of the inertial stabilization mechanism and the surface tension (the reactive force and the tension force). For small acceleration values, $0 < \tilde{G} < G_{cr}$, the buoyancy is dominated and the reactive and tension forces exceed the gravity. The solution is stable, and describes the standing wave stably oscillating in time. The flow dynamics is similar to the case of the inertial conservative dynamics with surface tension. For large acceleration values, $\tilde{G} > G_{cr}$, the buoyant effect dominates and the gravity exceeds the reactive and the tension forces. The solution is unstable, and describes the standing wave with the growing amplitude, figures 4, 5, tables 1, 5.

For given values of the density ratio and the surface tension, the solution is stable for $0 < G < \tilde{G}_{cr}$ and is unstable for $G > \tilde{G}_{cr}$, where the threshold value is $\tilde{G}_{cr} = R(R-1+T)/(R+1)$, with $\tilde{G}_{cr} \to G_{cr}$ for $T \to 0$. For given values of the density ratio and the acceleration, the solution is stable for $T > \tilde{T}_{cr}$, and is unstable for $T < \tilde{T}_{cr}$, where the critical surface tension value is $\tilde{T}_{cr} = (G(R+1) - R(R-1))/R$; it approaches $\tilde{T}_{cr} \to 0$ for $G \to G_{cr}^{+}$ and equals zero $\tilde{T}_{cr} = 0$ for $0 \leqslant G \leqslant G_{cr}$, figures 4, 5, 6, 7, tables 1, 5.

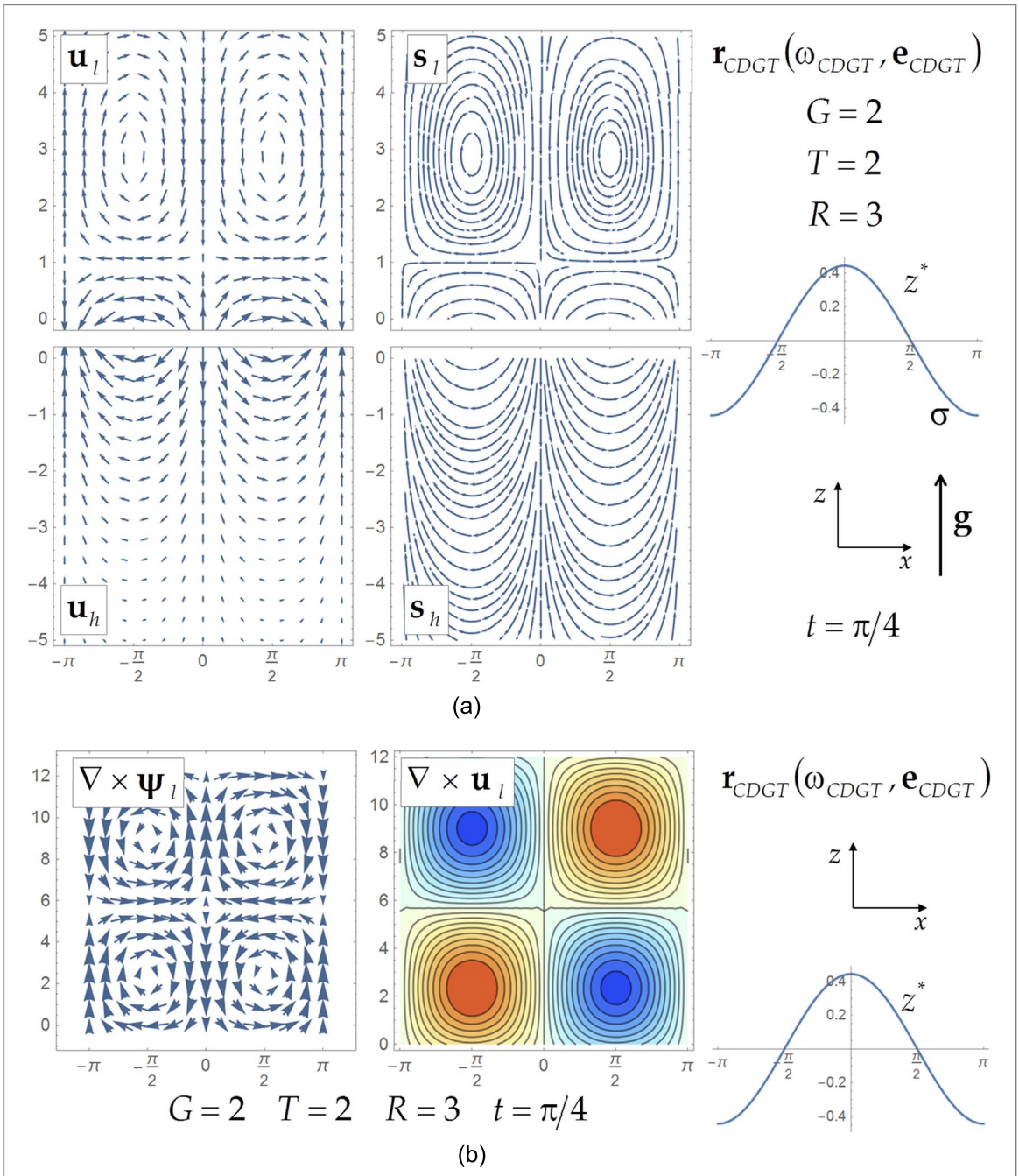

Figure 6. Flow fields for the fundamental solution for the accelerated conservative dynamics with surface tension in the stable regime at some instance of time and at some values of the density ratio, the acceleration, and the surface tension: (a) plots of the perturbed velocity vector fields, the perturbed velocity streamlines, and the interface perturbation; (b) plots of the vortical component of the perturbed velocity and the perturbed vorticity. Real parts of fields and functions are shown. Each plot has its own range of values to better present the plot's features.

Structure of the flow fields: Consider the structure of the flow fields for the solution $\mathbf{r}_{CDGT}$ equation (20), table 1, figures 6, 7. In this solution, in the limit of zero surface tension, $T \to 0$, the vortical component vanishes, $\psi \to 0$, and the accelerated conservative dynamics free from surface tension has potential velocity fields in the fluids' bulks [21, 22]. For a finite value of the surface tension, $T > 0$, in the solution $\mathbf{r}_{CDGT}$, the vortical component is finite, $\psi \neq 0$, equation (20), table 1, figures 6, 7. This accelerated conservative dynamics with surface tension has potential velocity field in the bulk of the heavy fluid, and the velocity field combining the potential and vortical components in the bulk of the light fluid. The appearance of the vortical field in the light fluid bulk is due to the surface energy contribution to the enthalpy jump at the interface $[w]$, and it defines the strength of the vortical field.

Stable dynamics: For $G < \tilde{G}_{cr}$ ($T > \tilde{T}_{cr}$) the accelerated conservative dynamics with surface tension $\mathbf{r}_{CDGT}$ is stable, equation (20), figures 4–6, tables 1, 5. In this regime, the eigenvalue ω_{CDGT} is purely imagine,

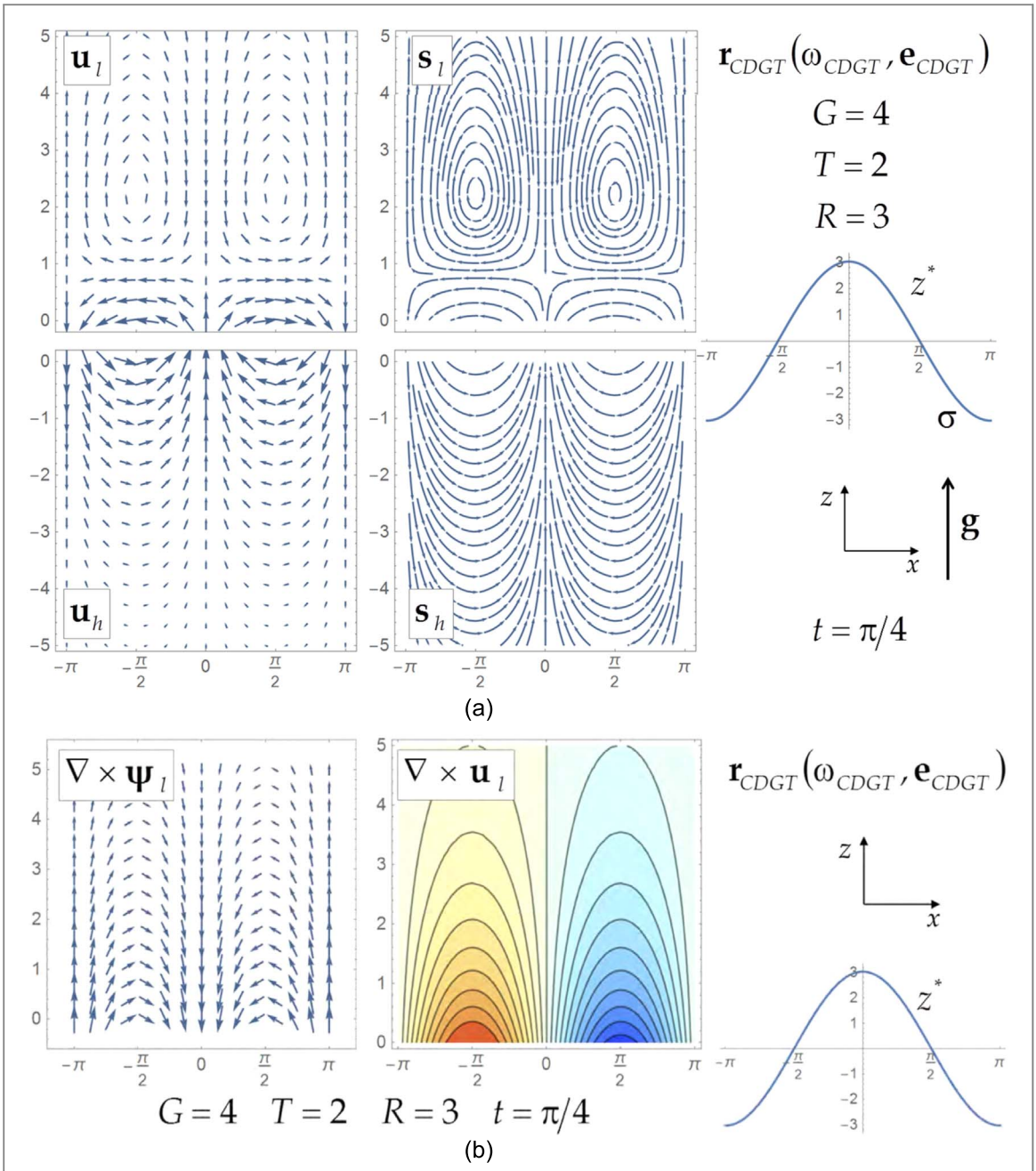

Figure 7. Flow fields for the fundamental solution for the accelerated conservative dynamics with surface tension in the unstable regime at some instance of time and at some values of the density ratio, the acceleration, and the surface tension: (a) plots of the perturbed velocity vector fields, the perturbed velocity streamlines, and the interface perturbation; (b) plots of the vortical component of the perturbed velocity and the perturbed vorticity. Real parts of fields and functions are shown. Each plot has its own range of values to better present the plot's features.

$\mathrm{Re}\,[\omega_{CDGT}] = 0$. The length-scale of the vortical field $\tilde{k} = (k/R)\ \omega_{CDGT}$ is also purely imagine, $\mathrm{Re}\,[\tilde{k}] = 0$. The solution $\mathbf{r}_{CDGT}$ is the standing wave stably oscillating in time, figure 6. In the heavy fluid bulk, the velocity field is potential; it is periodic in the x direction with the period $\lambda = 2\pi/k$ and decays away from the interface $z \to -\infty$. In the bulk of the light fluid, the velocity field combines the potential and the vortical components. The potential component is periodic in the x direction with period $\lambda = 2\pi/k$ and decays away from the interface $z \to +\infty$. The vortical component is periodic in the x direction with period $\lambda = 2\pi/k$, and is periodic in the z direction with period $\tilde{\lambda} = 2\pi/\tilde{k}$. The vorticity is $\nabla \times \mathbf{u}_l = (0,\ (1 - (\tilde{k}/k)^2)\psi_l,\ 0)$ and $\nabla \times \mathbf{u}_l \neq 0$, and the amplitude of this vortical structure is constant, figure 6.

In order for the solution $\mathbf{r}_{CDGT}$ to obey in the stable regime, $0 < G < \tilde{G}_{cr}$ the boundary condition $\mathbf{u}_l|_{z\to+\infty} = 0$, we are required to set its integration constant equal zero, $C_{CDGT}|_{G<\tilde{G}_{cr}} = 0$. Hence the perturbations are zero, and the interface velocity for this stable solution is constant $\tilde{\mathbf{V}} = \tilde{\mathbf{V}}_0$. Slight modifications of the boundary conditions away from the interface $z \to +\infty$ may lead to a non-zero integration constant

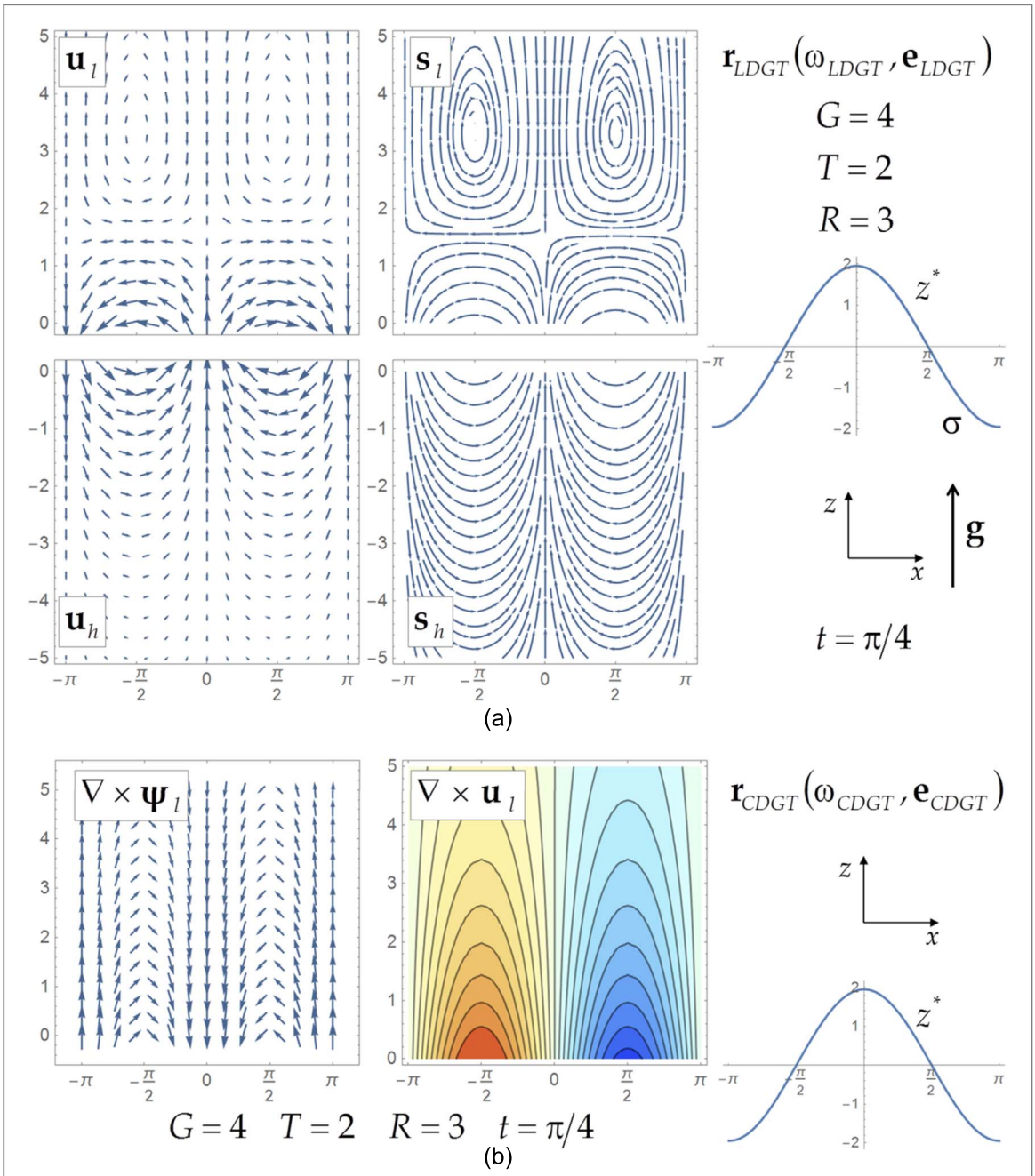

Figure 8. Flow fields for the fundamental solution for the accelerated Landau's dynamics with surface tension in the unstable regime of Landau-Darrieus instability at some instance of time and at some values of the density ratio, the acceleration, and the surface tension: (a) plots of the perturbed velocity vector fields, the perturbed velocity streamlines, and the interface perturbation; (b) plots of the vortical component of the perturbed velocity and the perturbed vorticity. Real parts of fields and functions are shown. Each plot has its own range of values to better present the plot's features.

$C_{CDGT}|_{G<\tilde{G}_{cr}}$. In this case, the interface velocity for the dynamics $\mathbf{r}_{CDGT}|_{G<\tilde{G}_{cr}}$ may slightly oscillate near a constant value, as $\tilde{\mathbf{V}} = \tilde{\mathbf{V}}_0 + \tilde{\mathbf{v}}$ with $\tilde{\mathbf{v}}\mathbf{n}_0 = -(\mathbf{u}_h\mathbf{n}_0 + \dot{\theta})|_{\theta=0} \sim e^{\pm i|\omega_{CDGT}|_{G=0}|\ t}$.

We see that in the stable regime, $G < \tilde{G}_{cr}$ ($T > \tilde{T}_{cr}$), the resultant accelerated conservative dynamics with surface tension may correspond to the stable unperturbed flow fields $(\rho,\ \mathbf{V},\ P_0,\ W_0)_{h(l)}$ and constant interface velocity $\tilde{\mathbf{V}} = \tilde{\mathbf{V}}_0$, figures 4–6, tables 1, 5. It may also exhibit stable oscillations of the interface and the interface velocity, as well as the velocity and the vorticity fields. In this case the buoyancy (the gravity) is dominated the combined effects of the inertial stabilization mechanism and the surface tension (the reactive force and the tension force).

Unstable dynamics: The accelerated conservative dynamics with surface tension $\mathbf{r}_{CDGT}$ is unstable for $G > \tilde{G}_{cr}$ ($T < \tilde{T}_{cr}$), figures 4, 5, 7, tables 1, 5. In this regime, the eigenvalue ω_{CDGT} is real and positive, $\mathrm{Re}\,[\omega_{CDGT}] > 0$ and $\mathrm{Im}[\omega_{CDGT}] = 0$. The dynamics $\mathbf{r}_{CDGT}$ couples the interface perturbation with the vortical and potential fields of the velocity $\nabla\varphi_h$, $\nabla\varphi_l$, $\nabla \times \boldsymbol{\psi}_l$. The potential and vortical components of the fluid

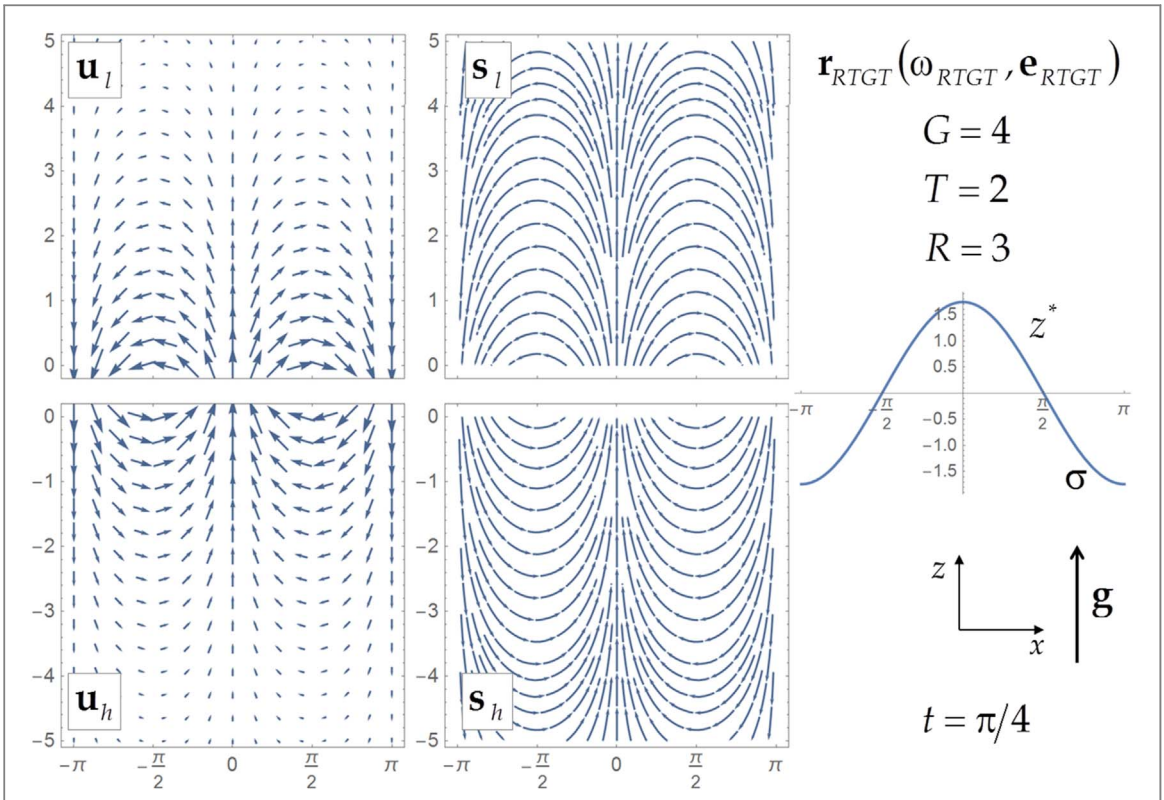

Figure 9. Flow fields for the fundamental solution for Rayleigh-Taylor dynamics with surface tension in Rayleigh-Taylor instability at some instance of time and at some values of the density ratio, the acceleration, and the surface tension: plots of the perturbed velocity vector fields, the perturbed velocity streamlines, and the interface perturbation. Real parts of fields and functions are shown. Each plot has its own range of values to better present the plot's features.

Table 5. Regions of stability and instability and critical parameters for the accelerated dynamics with the surface tension for the conservative, Landau's and Rayleigh-Taylor dynamics.

Dynamics	Stability region	Instability region	Critical values
$\mathbf{r}_{CDGT}$	$T > \tilde{T}_{cr}$	$T < \tilde{T}_{cr}$	$\tilde{T}_{cr} = \frac{G(R+1)-R(R-1)}{R}$
	$G < \tilde{G}_{cr}$	$G > \tilde{G}_{cr}$	$\tilde{G}_{cr} = R\frac{R-1}{R+1} + T\frac{R}{R+1}$
$\mathbf{r}_{LDGT}$	$T > \bar{T}_{cr}$	$T < \bar{T}_{cr}$	$\bar{T}_{cr} = \frac{(G+R)(R-1)}{R}$
	$G < \bar{G}_{cr}$	$G > \bar{G}_{cr}$	$\bar{G}_{cr} = T\frac{R}{R-1} - R$
$\mathbf{r}_{RTGT}$	$T > \hat{T}_{cr}$	$T < \hat{T}_{cr}$	$\hat{T}_{cr} = G\frac{(R-1)}{R}$
	$G < \hat{G}_{cr}$	$G > \hat{G}_{cr}$	$\hat{G}_{cr} = T\frac{R}{R-1}$

Table 6. Qualitative properties of the conservative, Landau's and Rayleigh-Taylor dynamics with the acceleration and surface tension in their corresponding stable and unstable regimes.

Dynamics	Regime	Interface velocity	Velocity fields	Interfacial shear
$\mathbf{r}_{CDGT}$	Stable	Constant	Unperturbed fields	Shear-free
	Unstable	Time-dependent	Potential and vortical components	Shear-free
$\mathbf{r}_{LDGT}$	Stable	Constant	Unperturbed fields	Shear-free
	Unstable	Constant	Potential and vortical components	Shear-free
$\mathbf{r}_{RTGT}$	Stable	Zero	Potential fields	Interfacial shear
	Unstable	Zero	Potential fields	Interfacial shear

velocities achieve their extreme values near the interface, and, while increasing in time, decay away from the interface.

The vortical field for the unstable solution $\mathbf{r}_{CDGT}$ with $G > \tilde{G}_{cr}$ ($T < \tilde{T}_{cr}$) in equation (20) has the following properties. The wavevector of the vortical field is $\tilde{k} = (k/R)\ \omega_{CDGT}$, and the length-scale of the vortical field is large

in a broad range of parameters, $(\tilde{k}/k) \ll 1$. When surface tension value decreases, $T \to 0$, the strength of the vortical field decreases, leading to the potential velocity fields are in the fluids' bulks, figures 4, 5, 7, tables 1, 5 [21, 22].

For the unstable accelerated conservative dynamics with surface tension, the buoyancy (the gravity) dominates the combined effects of the inertial stabilization mechanism and the surface tension (the reactive force and the tension force), figures 5, 7, tables 1, 5. For $G > \bar{G}_{cr}$ ($T < \bar{T}_{cr}$), the interface velocity of the solution $\mathbf{r}_{CDGT}$ increases with time, $\tilde{\mathbf{V}} = \tilde{\mathbf{V}}_0 + \tilde{\mathbf{v}}$ with $\tilde{\mathbf{v}}\mathbf{n}_0 \sim e^{|\omega_{CDGT}|\ t}$. The resultant flow is the superposition of two motions – the motion of the interface as whole with the growing interface velocity and the growth of the interface perturbations. The dynamics is shear free at the interface. When compared to the accelerated conservative dynamics free from surface tension, the surface tension influences the acceleration values at which the instability occurs, and also leads to the appearance of the vortical field in the bulk of the light fluid, figures 5, 7, tables 1, 5, [21, 22].

Summary: The accelerated conservative dynamics with surface tension can be stable of unstable depending on the values of the acceleration, the surface tension and the density ratio. In the stable regime, the resultant dynamics may have the stable unperturbed flow fields $(\rho,\ \mathbf{V},\ P_0,\ W_0)_{h(l)}$ and the constant interface velocity $\tilde{\mathbf{V}} = \tilde{\mathbf{V}}_0$ (and may also exhibit slight stable oscillations of the interface, the interface velocity, and the velocity and vorticity fields). In the unstable regime, the interface perturbations grow and so is the interface velocity. The dynamics couples the interface perturbation with the potential velocity field in the heavy fluid bulk and the potential and vortical components of the velocity field in the light fluid bulk, and is shear-free at the interface. The strength of the vortical field in the light fluid bulk depends on the surface tension; for zero surface tension, the velocity fields are potential in both fluids, figures 4, 5, 6, 7, tables 1, 5.

3.5.2. Classical Landau's dynamics

Fundamental solution: For the classical Landau's dynamics in the presence of acceleration and surface tension the solution is $\mathbf{r}_{LDGT} = \mathbf{r}_{LDGT}(\omega_{LDGT},\ \tilde{\mathbf{e}}_{LDGT})$ figures 4, 5, 8, tables 2, 5:

$$\omega_{LDGT} = \frac{-R + \sqrt{R^3 + R^2 - R + \bar{G}(R^2-1)}}{R+1}, \quad \mathbf{e}_{LDGT} = \mathbf{e} = (\varphi,\ \tilde{\varphi},\ 1,\ \psi)^T; \quad \bar{G} = G - \frac{T\ R}{R-1};$$
$$\tilde{\mathbf{V}} = \tilde{\mathbf{V}}_0 + \tilde{\mathbf{v}}, \quad \tilde{\mathbf{v}}\mathbf{n}_0 = -(\mathbf{u}_h\mathbf{n}_0 + \dot{\theta})|_{\theta=0} \equiv 0, \quad \tilde{\mathbf{V}} \equiv \tilde{\mathbf{V}}_0 \tag{21}$$

where the modified acceleration $\bar{G}$ accounts for the contribution of the surface tension T. The quantities $\{\varphi,\ \tilde{\varphi},\ \psi\}$ depend on the values of the density ratio, the acceleration and the surface tension $R,\ G,\ T$. For $T \to 0$ this solution is consistent with the solution for the accelerated Landau's dynamics free from surface tension equation (19.2), table 2 [20–22].

Stability and instability of the fundamental solution: In the classical Landau's dynamics the inertial stabilization mechanism is absent, due to the postulate of the constancy of the interface velocity. The dynamics can be stabilized by the surface tension. The solution $\mathbf{r}_{LDGT}$ is stable for $T > \bar{T}_{cr}$ ($G < \bar{G}_{cr}$) and is unstable for $T < \bar{T}_{cr}$ ($G > \bar{G}_{cr}$). The condition $\omega_{LDGT} = 0$ defines the critical values $\bar{T}_{cr} = (G+R)(R-1)/R$ and $\bar{G}_{cr} = (TR - R(R-1))/R$, figures 4, 5, tables 2, 5.

Structure of flow fields: In either stable or unstable regime, the dynamics $\mathbf{r}_{LDGT}$ couples the interface perturbation with the vortical and potential fields of the velocity $\nabla\varphi_h,\ \nabla\varphi_l,\ \nabla \times \boldsymbol{\psi}_l$. The presence of the vortical field in the classical Landau's dynamics is caused by the energy imbalance, which is due to the postulated constancy of the interface velocity $\tilde{\mathbf{V}} \equiv \tilde{\mathbf{V}}_0$ and the associated interfacial boundary condition for the perturbed velocity [21–23].

Stable dynamics: For $T > \bar{T}_{cr}$ ($G < \bar{G}_{cr}$), the solution is stable, with $\mathrm{Re}\,[\omega_{LDGT}] < 0$, and the length-scale of the vortical field $\tilde{k} = (k/R)\ \omega_{LDGT}$ has the negative real part $\mathrm{Re}\,[\tilde{k}] < 0$, figures 4, 5, tables 2, 5. The vortical component of the velocity of the light fluid $\nabla \times \boldsymbol{\psi}_l$ and its vorticity $\nabla \times \mathbf{u}_l = (0,\ (1 - (\tilde{k}/k)^2)\psi_l,\ 0)$ increase far from the interface, $z \to +\infty$. In order for the solution $\mathbf{r}_{LDGT}$ to obey the boundary condition $\mathbf{u}_l|_{z\to+\infty} = 0$ in equations (8.2), (12.1), we must set its integration constant equal zero $C_{LDGT} = 0$. Hence, in the stable regime, $T > \bar{T}_{cr}$ ($G < \bar{G}_{cr}$), the Landau's dynamics with the acceleration and the surface tension has unperturbed flow fields $(\rho,\ \mathbf{V},\ P_0,\ W_0)_{h(l)}$ and constant interface velocity .

Unstable dynamics: For $T < \bar{T}_{cr}$ ($G > \bar{G}_{cr}$) the accelerated Landau's dynamics with surface tension $\mathbf{r}_{LDGT}$ is unstable, equation (21), figures 4, 5, 8, tables 2, 5. In this regime, the eigenvalue ω_{LDGT} is real and positive, $\mathrm{Re}[\omega_{LDGT}] > 0$ and $\mathrm{Im}[\omega_{LDGT}] = 0$. The dynamics $\mathbf{r}_{LDGT}$ couples the interface perturbation with the vortical and potential fields of the velocity $\nabla\varphi_h,\ \nabla\varphi_l,\ \nabla \times \boldsymbol{\psi}_l$. The potential and vortical components of the fluid velocities achieve their maximum values near the interface, and, while increasing in time, decay away from the interface, figure 8. For the unstable solution $\mathbf{r}_{LDGT}$ with $T < \bar{T}_{cr}$ in equation (21), the vortical field has the wavevector $\tilde{k} = (k/R)\ \omega_{LDGT}$; the length-scale of the vortical field is large, $(\tilde{k}/k) \ll 1$, in a broad range of parameters. While the vortical field depends on the surface tension value, it is present for any values of the acceleration and the surface tension, and is associated with the energy imbalance for the Landau's dynamics

[21–23]. Hence, in the unstable regime, $T < \bar{T}_{cr}$ ($G > \bar{G}_{cr}$) the accelerated Landau's dynamics with surface tension is the superposition of two motions – the motion of the interface with the constant velocity $\tilde{\mathbf{V}} \equiv \tilde{\mathbf{V}}_0$ and the growth of the interface perturbations. It is shear free at the interface.

Summary: The accelerated Landau's dynamics with surface tension can be stable or unstable depending on the values of the acceleration, the surface tension and the density ratio. In the stable regime, the resultant dynamics corresponds to the stable unperturbed flow fields $(\rho,\ \mathbf{V},\ P_0,\ W_0)_{h(l)}$ and has constant interface velocity $\tilde{\mathbf{V}} \equiv \tilde{\mathbf{V}}_0$. In the unstable regime, the interface perturbations grow, whereas the interface velocity remains constant. The unstable dynamics couples the interface perturbation with the potential and vortical components of the velocity fields in the fluids' bulk, and is shear-free at the interface. The presence of the vortical field in the light fluid bulk is due to the postulated constancy of the interface velocity, leading to energy imbalance for any value of the acceleration and the surface tension, figures 4, 5, 8, tables 2, 5 [21–23].

3.5.3. Rayleigh-Taylor dynamics

Fundamental solution: For Rayleigh-Taylor dynamics in the presence of acceleration and surface tension the solution is $\mathbf{r}_{RDGT} = \mathbf{r}_{RDGT}(\omega_{RDGT},\ \tilde{\mathbf{e}}_{RDGT})$, figures 4, 5, 9, tables 3, 5

$$\begin{aligned}
&\bar{G} < 0, \quad \omega_{RTGT} = \pm i\sqrt{\bar{G}}\sqrt{\frac{R-1}{R+1}}, \quad \mathbf{e}_{RTGT} = \frac{\mathbf{e}+\mathbf{e}^*}{2}, \quad \mathbf{e} = (\varphi,\ \ \tilde{\varphi},\ \ 1)^T;\\
&\bar{G} > 0, \quad \omega_{RTGT} = \sqrt{\bar{G}}\sqrt{\frac{R-1}{R+1}}, \quad \mathbf{e}_{RTGT} = \mathbf{e} = (\varphi,\ \ \tilde{\varphi},\ \ 1)^T; \quad \bar{G} = G - \frac{T\ R}{R-1}
\end{aligned} \tag{22}$$

where the components of eigenvectors $\{\varphi,\ \ \tilde{\varphi}\}$ for solutions are the functions on $R,\ G,\ T$, table 3.

Stability and instability of the fundamental solution: Rayleigh-Taylor dynamics is stabilized by the surface tension. The solution $\mathbf{r}_{RTGT}$ is stable for $T > \hat{T}_{cr}$ and is unstable for $0 < T < \hat{T}_{cr}$. The critical surface tension value $\hat{T}_{cr} = G(R-1)/R$ is defined by the condition $\bar{G} = 0$, tables 3, 5; for $G \to 0$ the value approaches $\hat{T}_{cr} \to 0$, in agreement with equation (19.3).

Structure of flow fields In the stable and the unstable regimes of Rayleigh-Taylor dynamics with surface tension, the velocity fields are potential in the bulks of the light and the heavy fluid, and have the interfacial shear at the interface, figure 9.

Summary: For Rayleigh-Taylor dynamics with surface tension in the stable regime the dynamics describes the standing wave stably oscillating in time (which is the capillary wave for zero acceleration). In the unstable regime the dynamics describes the standing wave with the growing amplitude. The velocity fields are potential in the bulks of the light and the heavy fluid, and there is the shear at the interface, figure 9, table 3 [20–31]. The interface velocity is zero in the laboratory reference frame.

3.5.4. Summary of properties

Depending on the values of the acceleration, the surface tension and the density ratio, the dynamics $\{\mathbf{r}_{CDGT},\ \ \mathbf{r}_{LDGT},\ \ \mathbf{r}_{RTGT}\}$ can be stable or unstable, figures 4–9, tables 1–3, 5, 6. In either stable or unstable regime, these dynamics have distinct qualitative properties.

The accelerated conservative dynamics is stable (unstable) for $T > (<)\ \ \tilde{T}_{cr}$ and $G < (>)\ \ \tilde{G}_{cr}$. In the stable regime, the resultant motion corresponds to unperturbed flow fields with constant interface velocity and zero interfacial shear. In the unstable regime, the dynamics couples the interface perturbations with the potential and vortical components of the velocity fields in the fluids' bulks and is shear free at the interface; the interface perturbations grow with time and so is the interface velocity, figures 4–7, tables 1, 5, 6.

The accelerated Landau's dynamics is stable (unstable) for $T > (<)\ \ \bar{T}_{cr}$ and $G < (>)\ \ \bar{G}_{cr}$. In the stable regime, the resultant dynamics corresponds to unperturbed flow fields with constant interface velocity and with zero interfacial shear. In the unstable regime, the dynamics couples the interface perturbations with the potential and vortical components of the velocity fields in the fluids' bulks and is shear free at the interface; the interface perturbations grow with time; the interface velocity is constant, figures 4, 5, 8, tables 2, 5, 6.

Rayleigh-Taylor dynamics is stable (unstable) for $T > (<)\ \ \hat{T}_{cr}$ and $G < (>)\ \ \hat{G}_{cr}$. In either regime the dynamics has potential velocity fields in the fluid bulks and has the interfacial shear; the interface velocity is zero in the laboratory frame of reference. In the stable regime, the dynamics describes the stably oscillating standing wave. In the unstable regime, the amplitude of the standing wave grows with time, figures 4, 5, 9, tables 3, 5, 6.

3.5.5. Physics properties of mathematical attributes

For the accelerated dynamics, the interface stability and the structure of the flow fields are defined by the interfacial boundary conditions and by the interplay of the inertial effect, the surface tension and the acceleration. One may differentiate between various unstable dynamics and thus deduce the properties of the microscopic interfacial transport by measuring the macroscopic fields in the bulk. Particularly, the observations

of the vortex-free velocity fields in the bulk, the appearance of shear-driven vortical structures at the interface, and the zero interface velocity are indicative of the unstable Rayleigh-Taylor dynamics free from interfacial mass flux. The observations of the large-scale vortical field in the bulk, the absence of vortical structures at the interface and the constant interface velocity are indicative of Landau-Darrieus instability characterized by energy imbalance at the interface. The observations of the vortical field in the bulk, the absence of vortical structures at the interface and the growing interface velocity are indicative of the unstable accelerated conservative inertial dynamics. These results can be applied for design and interpretation of experimental and observational data.

3.6. Mechanisms of stabilization and destabilization

By comparing properties of fundamental solutions $\{\mathbf{r}_{CDGT},\ \mathbf{r}_{LDGT},\ \mathbf{r}_{RTGT}\}$ we further analyze the mechanisms of stabilization and destabilization of the interface dynamics influenced by the acceleration and surface tension, figures 4–9, tables 1–3, 5, 6.

3.6.1. Acceleration

Since the acceleration is directed from the heavy fluid to the light fluid, its qualitative role is to destabilize the interface dynamics. Quantitative effect of the acceleration is however distinct for the conservative, Landau's and Rayleigh-Taylor dynamics.

By comparing the growth-rates' values for the dynamics $\{\mathbf{r}_{CDGT},\ \mathbf{r}_{LDGT},\ \mathbf{r}_{RTGT}\}$, we find that at $T=0$ they are $\omega_{CDGT}=\omega_{LDGT}=\omega_{RTGT}$ at $G=G^*=(R^2-1)/4$. For strong accelerations and weak surface tension the dynamics $\{\mathbf{r}_{CDGT},\ \mathbf{r}_{LDGT},\ \mathbf{r}_{RTGT}\}$ are unstable, and the growth-rates behave as

$$
\begin{gathered}
G\to\infty,\quad T\to 0:\qquad \omega_{CDGT}>\omega_{LDGT}>\omega_{RTGT}\\
\omega_{CDGT}\to\sqrt{G}\sqrt{\frac{R+1}{R-1}}+\frac{1}{2\sqrt{G}}\left(-\frac{TR}{\sqrt{R^2-1}}-R\sqrt{\frac{R-1}{R+1}}\right);\\
\omega_{LDGT}\to\sqrt{G}\sqrt{\frac{1}{R+1}}+\left(-1+\frac{1}{R+1}\right)+\frac{1}{2\sqrt{G}}\left(-\frac{TR}{\sqrt{R^2-1}}+\frac{R(R^2+R-1)}{(R+1)\sqrt{R^2-1}}\right);\\
\omega_{RTGT}\to\sqrt{G}\sqrt{\frac{R-1}{R+1}}+\frac{1}{2\sqrt{G}}\left(-\frac{TR}{\sqrt{R^2-1}}\right)
\end{gathered}
\tag{23}
$$

Hence, in the limit of strong accelerations and weak surface tension values, the new fluid instability of the conservative dynamics has the largest growth-rate when compared to the accelerated Landau's and Rayleigh-Taylor dynamics, figure 5, tables 1–3.

3.6.2. Surface tension

The surface tension qualitative role is to stabilize the interface dynamics. Quantitative effect of the surface tension is however distinct for the conservative, Landau's and Rayleigh-Taylor dynamics.

For given values of the acceleration and density ratio $G>0$, $R>1$, each of the dynamics $\{\mathbf{r}_{CDGT},\ \mathbf{r}_{LDGT},\ \mathbf{r}_{RTGT}\}$ can be stabilized by surface tension. The new fluid instability of the accelerated conservative dynamics is stabilized for $T>\tilde{T}_{cr}$. The Landau's dynamics is stabilized for $T>\bar{T}_{cr}$. Rayleigh-Taylor dynamics is stabilized for $T>\hat{T}_{cr}$. By comparing the critical surface tension values for given values of the acceleration and the density ratio, we find (figures 4, 5, tables 1–3, 5): For $G>0,\quad R>1$ the values related as $\bar{T}_{cr}>\hat{T}_{cr}$, and the Landau's dynamics can be stabilized by larger surface tension when compared to Rayleigh-Taylor dynamics. For $G>R(R-1)/2$ the values relate as $\hat{T}_{cr}>\tilde{T}_{cr}$, and Rayleigh-Taylor dynamics can be stabilized by larger surface tension when compared to the new fluid instability of the conservative dynamics. For $G>R(R-1)$ the values relate as $\tilde{T}_{cr}>\hat{T}_{cr}$, and the Landau's dynamics can be stabilized by smaller surface tension when compared to the new fluid instability of the conservative dynamics, figures 4, 5, table 5.

Hence, for weak accelerations, $G<R(R-1)/2$, the critical surface tension values relate as $\tilde{T}_{cr}<\hat{T}_{cr}<\bar{T}_{cr}$ and the new fluid instability of the accelerated dynamics is stabilized by the smallest surface tension value when compare to Rayleigh-Taylor and Landau's dynamics. For intermediate accelerations, $R(R-1)/2<G<R(R-1)$ the values relate as $\hat{T}_{cr}<\tilde{T}_{cr}<\bar{T}_{cr}$. For strong accelerations, $G>R(R-1)$, the values relate as $\hat{T}_{cr}<\bar{T}_{cr}<\tilde{T}_{cr}$ and the new fluid instability of the conservative dynamics requires the largest surface tension value for the stabilization, when compared to Rayleigh-Taylor and Landau's dynamics, figures 4, 5, table 5.

3.6.3. Inertial stabilization mechanism

These results have clear physics interpretation: The conservative dynamics has inertial stabilization mechanism. Hence, for weak accelerations, the presence of this mechanism leads to smaller values of surface tension required for the interface stabilization, when compared to Landau's and Rayleigh-Taylor dynamics. For strong

Table 7. Value of critical wavevector for the conservative, Landau's and Rayleigh-Taylor dynamics.

$\mathbf{r}_{CDGT}$	$\tilde{k}_{cr}$	$\frac{1}{2\sigma}\left[-V_h^2\left(\frac{\rho_h}{\rho_l}\right)(\rho_h-\rho_l)+\sqrt{4\sigma g(\rho_h+\rho_l)+\left(V_h^2\left(\frac{\rho_h}{\rho_l}\right)(\rho_h-\rho_l)\right)^2}\right]$
$\mathbf{r}_{LDGT}$	$\bar{k}_{cr}$	$\frac{1}{2\sigma}\left[-V_h^2\left(\frac{\rho_h}{\rho_l}\right)(\rho_h-\rho_l)+\sqrt{4\sigma g(\rho_h-\rho_l)+\left(V_h^2\left(\frac{\rho_h}{\rho_l}\right)(\rho_h-\rho_l)\right)^2}\right]$
$\mathbf{r}_{RTGT}$	$\hat{k}_{cr}$	$\sqrt{\frac{g}{\sigma}(\rho_h-\rho_l)}$

Table 8. Value of maximum wavevector for the conservative, Landau's and Rayleigh-Taylor dynamics.

$\mathbf{r}_{CDGT}$	$\tilde{k}_{\max}$	$\frac{1}{6\sigma}\left[-2V_h^2\left(\frac{\rho_h}{\rho_l}\right)(\rho_h-\rho_l)+\sqrt{12\sigma g(\rho_h+\rho_l)+\left(2V_h^2\left(\frac{\rho_h}{\rho_l}\right)(\rho_h-\rho_l)\right)^2}\right]$
$\mathbf{r}_{LDGT}$	$\bar{k}_{\max}$	$\bar{k}_{\max}=\bar{k}_{\max}(V_h,\,g,\,\sigma,\,\rho_h,\,\rho_l)$
$\mathbf{r}_{RTGT}$	$\hat{k}_{\max}$	$\frac{1}{\sqrt{3}}\sqrt{\frac{g}{\sigma}(\rho_h-\rho_l)}$

accelerations, the conservative dynamics has the largest growth-rate leading to the largest surface tension value required for the interface stabilization, when compared to Landau's and Rayleigh-Taylor dynamics.

The inertial stabilization mechanism is the new mechanism recently discovered for the interface dynamics with interfacial mass flux [21, 22]. This mechanism is the essential property of the dynamics at macroscopic continuous scales. It is associated with the conservation of momentum and energy in the fluid system [21, 22]. It is exhibited in the non-constancy of the interface velocity for the unsteady non-planar interface. This mechanism is absent in the classical Landau's dynamics due to the postulated constancy of the interface velocity. It is also absent in Rayleigh-Taylor dynamics, in which the interface velocity is zero in the laboratory frame of reference.

In the stable regime, the inertial stabilization mechanism is revealed in slight oscillations of the interface velocity at zero surface tension (or at some noisy boundary conditions away from the interface). In the unstable regime, its presence is exhibited in the non-constancy of the interface velocity.

3.7. Characteristic length scales

The values of gravity g, the velocity V_h, the surface tension σ and the fluid densities $\rho_{h(l)}$ define the characteristic length-scales and time-scales of the dynamics of ideal incompressible fluids. These include the critical value of the wavevector k_{cr} at which the interface is stabilized, and the maximum value of the wavevector $k_{\max}$ at which the maximum value is achieved of the growth-rate of the interface perturbations, and the associated length-scales (wavelengths) $\lambda_{cr(\max)}=2\pi/k_{cr(\max)}$ and time-scales $\tau_{cr(\max)}=(k_{cr(\max)}V_h)^{-1}$. For given values of V_h, g, σ, ρ_h, ρ_l, we present in the dimensional form each of the dynamics $\{\mathbf{r}_{CDGT},\ \mathbf{r}_{LDGT},\ \mathbf{r}_{RTGT}\}$ and find the critical and the maximum wavevector values from the conditions (tables 7, 8):

$$\Omega|_{k=k_{cr}}=0;\quad \left.\frac{\partial\Omega}{\partial k}\right|_{k=k_{\max}}=0,\quad \left.\frac{\partial^2\Omega}{\partial k^2}\right|_{k=k_{\max}}<0;\quad \Omega=\Omega_{CDGT\,(LDGT)(RTGT)} \tag{24}$$

The information on these scales is critical for design of experiments and simulations, since it ensures the sufficient resolution of the observational results [20].

Conservative dynamics: For the fundamental solution $\mathbf{r}_{CDGT}$ with $\Omega=\Omega_{CDGT}$ in equation (24), the critical and the maximum wavevector values are (tables 7, 8):

$$\Omega_{CDGT}|_{k=\tilde{k}_{kr}}=0;\quad \left.\frac{\partial\Omega_{CDGT}}{\partial k}\right|_{k=\tilde{k}_{\max}}=0,\quad \left.\frac{\partial^2\Omega_{CDGT}}{\partial k^2}\right|_{k=\tilde{k}_{\max}}<0$$

$$\tilde{k}_{cr}=\frac{1}{2\sigma}\left[-V_h^2\left(\frac{\rho_h}{\rho_l}\right)(\rho_h-\rho_l)+\sqrt{4\sigma g(\rho_h+\rho_l)+\left(V_h^2\left(\frac{\rho_h}{\rho_l}\right)(\rho_h-\rho_l)\right)^2}\right]$$

$$\tilde{k}_{\max}=\frac{1}{6\sigma}\left[-2V_h^2\left(\frac{\rho_h}{\rho_l}\right)(\rho_h-\rho_l)+\sqrt{12\sigma g(\rho_h+\rho_l)+\left(2V_h^2\left(\frac{\rho_h}{\rho_l}\right)(\rho_h-\rho_l)\right)^2}\right] \tag{25.1}$$

For $|\sigma g(\rho_h+\rho_l)/(V_h^2(\rho_h/\rho_l)(\rho_h-\rho_l))^2| \to 0$ the values $\tilde{k}_{cr(\max)}/(g/V_h^2) \sim O(1)$ remain finite, whereas for $|\sigma g(\rho_h+\rho_l)/(V_h^2(\rho_h/\rho_l)(\rho_h-\rho_l))^2| \to \infty$ the values approach $\tilde{k}_{cr(\max)}/(g/V_h^2) \to 0$.

The ratio $(\tilde{k}_{cr}/\tilde{k}_{\max})$ is the function on the parameters V_h, g, σ, ρ_h, ρ_l, tables 7, 8. For vanishing surface tension, the critical and maximum wave-vector values and their ratio are:

$$\left|\frac{\sigma}{V_h^2(\rho_h-\rho_l)}\frac{g}{V_h^2}\left(\frac{\rho_h+\rho_l}{\rho_h-\rho_l}\right)\left(\frac{\rho_h}{\rho_l}\right)^2\right| \to 0;$$
$$\tilde{k}_{cr} \to \frac{g}{V_h^2}\frac{\rho_l}{\rho_h}\left(\frac{\rho_h+\rho_l}{\rho_h-\rho_l}\right)\cdots; \quad \tilde{k}_{\max} \to \frac{1}{2}\frac{g}{V_h^2}\frac{\rho_l}{\rho_h}\left(\frac{\rho_h+\rho_l}{\rho_h-\rho_l}\right); \quad \frac{\tilde{k}_{cr}}{\tilde{k}_{\max}} \to 2 \tag{25.2}$$

For very large surface tension, the critical and maximum wave-vector values and their ratio are:

$$\left|\frac{\sigma}{V_h^2(\rho_h-\rho_l)}\frac{g}{V_h^2}\left(\frac{\rho_h+\rho_l}{\rho_h-\rho_l}\right)\left(\frac{\rho_h}{\rho_l}\right)^2\right| \to \infty$$
$$\tilde{k}_{cr} \to \sqrt{\frac{g(\rho_h+\rho_l)}{\sigma}}; \quad \tilde{k}_{\max} \to \frac{1}{\sqrt{3}}\sqrt{\frac{g(\rho_h+\rho_l)}{\sigma}}; \quad \frac{\tilde{k}_{cr}}{\tilde{k}_{\max}} \to \sqrt{3} \tag{25.3}$$

Classical Landau's dynamics: For the fundamental solution $\mathbf{r}_{LDGT}$ with $\Omega = \Omega_{LDGT}$ equation (24), the critical and maximum wavevector values are (tables 7, 8):

$$\Omega_{LDGT}|_{k=\bar{k}_{kr}} = 0; \quad \left.\frac{\partial\Omega_{LDGT}}{\partial k}\right|_{k=\bar{k}_{\max}} = 0, \quad \left.\frac{\partial^2\Omega_{LDGT}}{\partial k^2}\right|_{k=\bar{k}_{\max}} < 0$$
$$\bar{k}_{cr} = \frac{1}{2\sigma}\left[-V_h^2\left(\frac{\rho_h}{\rho_l}\right)(\rho_h-\rho_l) + \sqrt{4\sigma g(\rho_h-\rho_l)+\left(V_h^2\left(\frac{\rho_h}{\rho_l}\right)(\rho_h-\rho_l)\right)^2}\right]$$
$$\bar{k}_{\max} = \bar{k}_{\max}(V_h, g, \sigma, \rho_h, \rho_l) \tag{26.1}$$

For vanishing surface tension values $|\sigma g/(V_h^4(\rho_h/\rho_l)^2(\rho_h-\rho_l))| \to 0$ the critical and maximum wave-vectors values approach $\bar{k}_{cr(\max)}/(g/V_h^2) \to \infty$, whereas for $|\sigma g/(V_h^4(\rho_h/\rho_l)^2(\rho_h-\rho_l))| \to \infty$, the values are $\bar{k}_{cr(\max)}/(g/V_h^2) \to 0$.

The ratio $(\bar{k}_{cr}/\bar{k}_{\max})$ is a cumbersome function on the parameters V_h, g, σ, ρ_h, ρ_l, tables 7, 8. For vanishing surface tension, the critical and maximum wave-vector values and their ratio are:

$$\left|\frac{\sigma}{V_h^2(\rho_h-\rho_l)}\frac{g}{V_h^2}\left(\frac{\rho_h}{\rho_l}\right)^2\right| \to 0; \qquad \bar{k}_{cr} \to \frac{\rho_h V_h^2}{\sigma}\left(\frac{\rho_h}{\rho_l}\right)\left(1-\frac{\rho_l}{\rho_h}\right);$$
$$\bar{k}_{\max} \to \frac{\rho_h V_h^2}{\sigma}s\left(\frac{\rho_h}{\rho_l}\right), \quad s|_{\frac{\rho_h}{\rho_l}\to 1^+} \to \frac{1}{2}\left(1-\left(\frac{\rho_l}{\rho_h}\right)\right), \quad s|_{\frac{\rho_h}{\rho_l}\to\infty} \to \frac{2}{3}\left(\frac{\rho_h}{\rho_l}\right);$$
$$\left.\frac{\bar{k}_{cr}}{\bar{k}_{\max}}\right|_{\frac{\rho_h}{\rho_l}\to 1^+} \to 2, \qquad \left.\frac{\bar{k}_{cr}}{\bar{k}_{\max}}\right|_{\frac{\rho_h}{\rho_l}\to\infty} \to \frac{3}{2} \tag{26.2}$$

For very large surface tension, the critical and maximum wave-vector values and their ratio are:

$$\left|\frac{\sigma}{V_h^2(\rho_h-\rho_l)}\frac{g}{V_h^2}\left(\frac{\rho_h}{\rho_l}\right)^2\right| \to \infty; \qquad \bar{k}_{cr} \to \sqrt{\frac{g(\rho_h-\rho_l)}{\sigma}};$$
$$\bar{k}_{\max} \to \sqrt{\frac{g(\rho_h-\rho_l)}{\sigma}}p\left(\frac{\rho_h}{\rho_l}\right), \quad p|_{\frac{\rho_h}{\rho_l}\to 1^+} \to \frac{1}{\sqrt{3}}\sqrt{\frac{\rho_h}{\rho_l}-1}, \quad p|_{\frac{\rho_h}{\rho_l}\to\infty} \to \frac{1}{\sqrt{3}}$$
$$\left.\frac{\bar{k}_{cr}}{\bar{k}_{\max}}\right|_{\frac{\rho_h}{\rho_l}\to 1^+} \to \sqrt{3}, \qquad \left.\frac{\bar{k}_{cr}}{\bar{k}_{\max}}\right|_{\frac{\rho_h}{\rho_l}\to\infty} \to \sqrt{3} \tag{26.3}$$

Rayleigh-Taylor dynamics: For the fundamental solution $\mathbf{r}_{RTGT}$ with $\Omega = \Omega_{RTGT}$ in equation (24), the critical and the maximum wavevector values are (tables 7, 8):

$$\Omega_{RTGT}|_{k=\hat{k}_{cr}}=0;\quad \left.\frac{\partial\Omega_{RTGT}}{\partial k}\right|_{k=\hat{k}_{\max}}=0,\quad \left.\frac{\partial^2\Omega_{RTGT}}{\partial k^2}\right|_{k=\hat{k}_{\max}}<0$$
$$\hat{k}_{cr}=\sqrt{\frac{g}{\sigma}(\rho_h-\rho_l)};\quad \hat{k}_{\max}=\frac{1}{\sqrt{3}}\sqrt{\frac{g}{\sigma}(\rho_h-\rho_l)};\quad \frac{\hat{k}_{cr}}{\hat{k}_{\max}}=\sqrt{3} \tag{27}$$

For vanishing surface tension values, $|\sigma/(g(\rho_h-\rho_l))|\to 0$, the critical and maximum wavevector values approach $\hat{k}_{cr(\max)}/(g/V_h^2)\to\infty$, whereas for very large surface tension values $|\sigma/(g(\rho_h-\rho_l))|\to\infty$ the critical and maximum wavevector values approach $\hat{k}_{cr(\max)}/(g/V_h^2)\to 0$ for given finite values of g, V_h, where V_h is understood as some velocity scale. The ratio of the critical and maximum wavevector values is $(\hat{k}_{\max}/\hat{k}_{cr})=1/\sqrt{3}$ for any $|\sigma/(g(\rho_h-\rho_l))|>0$, tables 7, 8.

Comparative analysis: The conservative dynamics of the fluid interface is stabilized by the inertial mechanism and by the surface tension, and is destabilized by the acceleration. The presence of the inertial stabilization mechanism is revealed in the finite values of the critical and the maximum wavevector values $\tilde{k}_{cr(\max)}/(g/V_h^2)\sim O(1)$ in the limit of vanishing surface tension. For very large surface tension values the critical and the maximum wavevector values approach zero $\tilde{k}_{cr(\max)}/(g/V_h^2)\to 0$. The ratio $(\tilde{k}_{cr}/\tilde{k}_{\max})$ is the function on the parameters V_h, g, σ, ρ_h, ρ_l, and it varies from 2 to $\sqrt{3}$ with the increase of the surface tension parameter $|\sigma g(\rho_h+\rho_l)/(V_h^2(\rho_h/\rho_l)(\rho_h-\rho_l))^2|$ from zero to infinity, tables 7, 8.

In the Landau's and Rayleigh-Taylor dynamics the properties of the characteristic scales are distinct when compared to those in the conservative dynamics, tables 7, 8. The Landau's dynamics is stabilized by surface tension, and it is unstable even for zero acceleration. For given values of g, V_h, in the limit of vanishing surface tension values the critical and maximum wavevector values approach $\bar{k}_{cr(\max)}/(g/V_h^2)\to\infty$. For very large surface tension values, the critical and maximum wavevector values approach $\bar{k}_{cr(\max)}/(g/V_h^2)\to 0$. The ratio $(\bar{k}_{cr}/\bar{k}_{\max})$ depends on the density ratio (ρ_h/ρ_l) and the surface tension parameter $|\sigma g/(V_h^4(\rho_h/\rho_l)^2(\rho_h-\rho_l))|$. With the increase of this parameter the ratio $(\bar{k}_{cr}/\bar{k}_{\max})$ varies from 2 for $(\rho_h/\rho_l)\sim 1$ and 3/2 for $(\rho_h/\rho_l)\gg 1$ to $\sqrt{3}$ for any density ratio (ρ_h/ρ_l), tables 7, 8.

Rayleigh-Taylor dynamics is stabilized by surface tension and is destabilized by the acceleration. For vanishing surface tension values, the critical and maximum wavevector values approach $\hat{k}_{cr(\max)}/(g/V_h^2)\to\infty$, whereas for very large surface tension values the critical and maximum wavevector values approach $\hat{k}_{cr(\max)}/(g/V_h^2)\to 0$, where V_h is some velocity scale. The ratio of the critical and maximum wavevector values is $(\hat{k}_{cr}/\hat{k}_{\max})=\sqrt{3}$ for any value of the surface tension parameter $|\sigma/(g(\rho_h-\rho_l))|>0$, tables 7, 8.

We thus conclude that the boundary conditions at the interface strongly influence the characteristic wavevectors, length-scales and time-scales of the interfacial dynamics. This information is critical for design of experiments and simulations. For instance, one may employ in experiments and simulations the dependence of the critical length- and time-scales on the acceleration strength and the surface tension in order to ensure that the observations are well resolved. One may also vary the initial perturbation wavelength and identify the length-scales corresponding to the stabilization and the fastest growth of the interface, and thus identify the properties of microscopic transport at the interface.

3.8. Outcome for experiments and simulations

Our analysis identifies the mechanisms of stabilization and destabilization of the interface dynamics with the interfacial mass flux and finds that the properties of the inertial and accelerated conservative dynamics with surface tension differ qualitatively and quantitatively from those of classical Landau's dynamics for Landau-Darrieus instability and Rayleigh-Taylor dynamics for Rayleigh-Taylor instability [21]. This opens new opportunities for experiments and simulations, and enables a better understanding and, ultimately, control of a broad range of processes in nature and technology to which unstable interfaces and interfacial mixing are relevant [1–45]. In this section we outline the outcomes of our analysis for experiments and simulations.

In order to compare with existing experiments and simulations, we note that our results for the Landau's dynamics and Rayleigh-Taylor dynamics agree with the results of theoretical, experimental and numerical studies [24–35, 46]. Furthermore, our results for the conservative dynamics clearly indicate that the interface can be stable even for ideal incompressible fluids with vanishing surface tension, when the acceleration value is smaller than a threshold, similarly to ablative Rayleigh-Taylor instabilities in high energy density plasmas [36–40, 46]. Another possible application of our results in multiphase geophysical flows is the stability of the interface between the oceans - when waters in the Pacific and Atlantic oceans meet and not mix at global scale [61].

Our theory elaborates extensive benchmark for future experiments and simulations. According to our results, for given values of the fluid densities $\rho_{h(l)}$ and the velocity V_h, in the regime of strong accelerations g, the new fluid instability of the conservative dynamics has the largest stabilizing surface tension σ and the largest

growth-rate Ω, when compared to the cases of the accelerated Landau's and Rayleigh-Taylor dynamics, equations (11), (12), (14), figures 5, 7, tables 1, 5, 6. The new fluid instability is the fastest in the extreme regimes of strong accelerations and weak surface tension, occurring, for instance in high energy density plasmas [5–9]. Hence, for given values of the parameters V_h, $\rho_{h(l)}$, σ, one can observe the new fluid instability by increasing the acceleration values. One can further observe that for the unstable accelerated conservative dynamics with surface tension, the growth of the interface perturbations is augmented with the growth of the interface velocity. The former is present and the latter is absent in Landau-Darrieus and Rayleigh-Taylor instabilities figure 7, table 6 [24–35]. By accurately diagnosing the interface dynamics, including the growth of the interface perturbations and the interface velocity, one can confidently find the new fluid instability in experiments with strong accelerations [5–9].

In some experiments the parameters of the dynamics V_h, g, σ, ρ_h, ρ_l may be a challenge to vary systematically [5–9, 39, 40]. Our analysis proposes how to address the challenge. Particularly, for given values of the parameters V_h, $\rho_{h(l)}$, σ, g, by varying the wavelength of the initial perturbation λ, one may observe the interface stabilization at the wavevector $k = k_{cr}$ and the fastest growth-rate of the unstable interface at the wavevector $k = k_{\max}$ and the associated length-scales $\lambda_{cr(\max)} = 2\pi/k_{cr(\max)}$ and time-scales $\tau_{cr(\max)} = (k_{cr(\max)} V_h)^{-1}$. One can further identify the type of the fluid instability, and differentiate between the new fluid instability of the conservative dynamics and the instabilities of the Landau's and Rayleigh-Taylor dynamics by comparing the critical and maximum scales $\lambda_{cr(\max)}$, $\tau_{cr(\max)}$ with the theoretical results for given values of the parameters, V_h, $\rho_{h(l)}$, σ, g, equations (25)–(27), tables 7, 8. These results can be applied for design of experiment in high energy density plasmas [5–9, 39, 40].

Our results indicate a need in further advancements of numerical modeling of the interface dynamics [41–43]. Numerical modeling of unstable fluid interfaces is a challenge because the simulations are required to track the interface, to capture small scales dissipative processes, and to use the highly accurate numerical methods and massive computations [1]. Existing numerical approaches usually apply diffusive approximation for modeling interfaces with interfacial mass flux, and work well for flows with smoothly changing of flow fields [2]. Our results indicate that new developments are required to accurately model the unstable interface with sharply changing flow fields, including the Lagrangian and Eulerian methods [1, 2, 41–43].

The existing experimental and numerical studies of the interface stability are focused on the measurements of the growth and growth-rate of the perturbation amplitude [2, 5–7, 39–43]. We derive the amplitude growth and the growth-rate, and we finds that the flow dynamics is highly sensitive to the interfacial boundary conditions, figures 2–9, tables 1–8. Our analysis directly links the macroscopic flow fields to the microscopic transport at the interface. It suggests that by measuring the flow fields at macroscopic scales in the bulk far from the interface, one can confidently capture the transport properties at microscopic scales at the interface, figures 2–8. This information is especially important for systems where experimental data are a challenge to obtain, including fusion, supernovae and scramjets [2–15].

Consider, for instance, the theory outcome for high energy density plasmas. In our analysis acceleration is a body force, and the acceleration magnitude is set constant in order to simplify the analysis equations (1–27). In experiments in laser-ablated plasmas the acceleration is an effective acceleration, and it is time-dependent; model experiment with a (quasi-) constant acceleration is extremely challenging to set up and conduct since it is the target, the laser-drive and the experiment specific [5–8]. Our analysis finds that for the unstable accelerated conservative dynamics, the interface velocity is a function of time even when the acceleration is constant. This is due to the conservation of mass, momentum and energy in the system. The time-dependence of the interface velocity can be exponential in the linear regime and a power-law in the nonlinear regime [21–23, 46]. In a frame of reference moving with the interface velocity, the system may experience an effective acceleration, which is a complex function of time and which may also depend on perturbation amplitude. While this opens exciting perspectives for theory research, it also indicates that the dynamics of unstable accelerated interfaces with interfacial mass flux, such as in laser-ablated plasmas and in type-Ia supernova [4–8], may be even more challenging than they may appear.

This suggests a need in new experimental approaches, that, on the one hand, would employ a striking similarity of non-equilibrium dynamics of interfaces and mixing in the vastly different physical regimes [1, 2], and, on the other hand, would be affordable and repeatable in a broad range of parameters, and conditions. In classical Rayleigh-Taylor instabilities, such approach was employed in jelly experiments and enabled the direct observation of the order in interfacial mixing at very high Reynolds numbers [28]. In laser-matter interactions, the experiments [9] provided observations of complex and ordered fine scale structures in Rayleigh-Taylor unstable interfaces. In classical plasmas the Large Plasma Device (LAPD) experiments [62] enabled the discovery of the spiky structures in magnetic flux ropes through scrupulous analysis of immense high quality data. In liquids, the experiments on liquid-liquid interfaces [63] provided the nano-scale view of assisted ion transport across the interface and revealed essentially non-diffusive interfacial transport. The theory and the experiments

suggest that the problem is the interface dynamics with interfacial mass flux is well open for curious mind [1, 2, 5–9, 28, 62, 63].

It is traditionally believed that the interface dynamics can be stabilized by factors depending on microscopic properties of matter (plasmas, fluids, materials), such as surface tension, diffusion, and dissipation, which, in turn, occur due to interactions of the constituting particles (atoms, molecules) [20, 30–35]. Our analysis suggests that while these factors indeed play a stabilizing role, the conservative dynamics of the interface with interfacial mass flux can also be stabilized by the inertial mechanism, which is enabled by the macroscopic motion of the interface as whole equations (11), (20) [21, 22]. This mechanism is absent in the classical Landau's dynamics, due to the postulated constancy of the interface velocity, and in Rayleigh-Taylor dynamics, where the interface velocity is zero in laboratory frame of reference equations (12), (14), (21), (22) [20–22]. In case of the accelerated dynamics with surface tension, the inertial mechanism is exhibited in the larger (smaller) values of surface tension required to stabilize the strongly (weakly) accelerated interface in the conservative dynamics when compared to the Landau's and Rayleigh-Taylor dynamics, figures 3–9, tables 1–5.

4. Discussion and conclusion

We investigated the interfacial dynamics with interfacial mass flux in the presence of the acceleration and the surface tension equations (1)–(27). We considered ideal and incompressible fluids with negligible stratification and densities variation for the two-dimensional spatially extended periodic flow with the acceleration directed from the heavy to the light fluid and with surface tension understood as the tension at the boundary between the flow phases. The general matrix method was advanced and applied to rigorously solve the linearized boundary value problem. The fundamental solutions were found for the dynamics conserving mass, momentum and energy, and were compared with those for the classical Landau's and Rayleigh-Taylor dynamics. The interplay of the acceleration, surface tension and inertial stabilization mechanism was scrupulously studied and its effect of the interface stability and on the properties of the new fluid instability of the conservative dynamics was identified. Extensive benchmarks were elaborated for future experiments and simulations and for better understanding of natural and technological processes, to which unstable interfaces are relevant, equations (1)–(27), figures 1–9, tables 1–8.

We found that the dynamics conserving mass, momentum and energy can be stable or unstable depending on the acceleration and the surface tension. In the stable regime, the conservative dynamics corresponds to non-perturbed flow fields in the bulk, is shear-free at the interface and has the constant interface velocity. The instability can develop only in the presence of the acceleration and only when its magnitude exceeds a threshold, equation (20), figures 2–7, tables 1, 4, 5, 6. This threshold value reflects the contributions of the inertial stabilization mechanism and the surface tension and is finite for zero surface tension. In the unstable regime, the interface perturbations are coupled with the potential and vortical components of the velocity fields in the fluids' bulk; for zero surface tension, the velocity fields are potential. The dynamics is shear-free at the interface. It describes the standing wave with the growing amplitude, and has the growing interface velocity, figure 6. Depending on the acceleration and the surface tension, the fluid instability of the conservative dynamics can grow faster or slower when compared to the accelerated Landau's and Rayleigh-Taylor dynamics; it has the largest growth-rate and the largest stabilizing surface tension value in the extreme regime of strong accelerations, equations (20)–(22), figures 4–9, tables 2–6. We also found the critical and maximum values of the wavevector of the initial perturbation at which the conservative instability is stabilized and at which it has the largest growth-rate, tables 7, 8. These unique quantitative and qualitative properties of the instability of the conservative dynamics clearly distinct it from other fluid instabilities, and call for further investigations, equations (1)–(27), figures 1–9, tables 1–8.

Our results agree qualitatively with available observations and indicate a strong need in further experimental and numerical studies of the interface dynamics, and in the development of new methods of numerical modeling and experimental diagnostics. Existing experimental and numerical studies of the interface dynamics are focused on diagnostics of the growth of the amplitude of the initial perturbation [1, 2, 39–43]. Our analysis provides the amplitude growth-rate in a broad range of parameters, determines the regions of the experimental parameter of the stable and unstable dynamics, identifies the structure of the flow field and links them to the boundary conditions at the interface equations (1)–(27), figures 1–9, tables 1–8. Particularly, according to our results, by measuring at macroscopic scales the flow fields in the bulk, one can capture the transport properties at microscopic scales at the interface, figures 6–9, table 6.

An important outcome of our theory for applied scientists and engineers is that for the interface dynamics with interfacial mass flux the interface unsteadiness and the interface stability are distinct concepts, equations (1)–(27). Indeed, for the accelerated conservative dynamics, due to the inertial stabilization mechanism, the interface velocity is unsteady in both stable and unstable regimes: It experiences slight

oscillations in the stable regime, and it increases with time in the unstable regime. This suggests that more caution is required with how the acceleration is defined: For the accelerated conservative dynamics with the interfacial mass flux the acceleration can be caused by the body force and be directed from the heavy to the light fluid in the inertial frame of reference. For Rayleigh-Taylor dynamics with zero interfacial mass flux, the acceleration can also be the acceleration of the fluid interface and be directed from the light to the heavy fluid in the inertial frame of reference, figures 1–9.

Our approach resolved the long-standing prospect of Landau [32], by showing that Landau's solution for Landau-Darrieus instability is a perfect mathematical match [21–23, 46]. Our results can be further connected to realistic environments in plasmas, fluids and material, in which the dynamics is usually accompanied by dissipation, diffusion, compressibility, radiation transport, stratification, and non-local forces, figures 1–9 [2–15]. Our general theoretical approach can be extended to systematically incorporate these effects, to analyze the interplay of the interface stability with the structure of flow fields, and to elaborate a unified theory framework for studies of interfacial dynamics in a broad range of processes including ablative Rayleigh-Taylor instabilities in fusion plasmas, dynamics of reactive and super-critical fluids, and D'yakov-Kontorovich instability of shock waves [1–45]. We address these studies to the future.

Acknowledgments

The authors thank for support the National Science Foundation (USA), award 1404449; the University of Western Australia (AUS), project grant 10101047; the Office of Naval Research (USA), grant N00014-19-1-2081.

Data availability statement

The data that support the findings of this study are available upon reasonable request from the authors.

Author's contributions

SIA designed research; DVI, SIA performed research; DVI, SIA analyzed data; DVI, WAG, IIA, SIA discussed results; DVI, SIA wrote the paper.

ORCID iDs

S I Abarzhi https://orcid.org/0000-0002-8466-3084

References

[1] Abarzhi S I and Goddard W A 2019 Interfaces and mixing: non-equilibrium transport across the scales *Proc. Natl Acad. Sci. USA* **116** 18171
[2] Abarzhi S I, Gauthier S and Sreenivasan K R 2013 Turbulent mixing and beyond: non-equilibrium processes from atomistic to astrophysical scales. I, II. Royal Society Publishing
[3] Arnett D 1996 *Supernovae and Nucleosynthesis.* (Princeton, NJ: Princeton University Press)
[4] Bell J B, Day M S, Rendleman C A, Woosley S E and Zingale M A 2004 Direct numerical simulations of type Ia supernovae flames I: The Landau-Darrieus instability. Astroph J 606, 1029; 2004 Direct numerical simulations of type Ia supernovae flames II: The Rayleigh-Taylor Instability *Astroph J* **608** 883
[5] Hurricane O A *et al* 2014 The high-foot implosion campaign on the National Ignition Facility *Phys. Plasmas* **21** 056314
[6] Haan S W *et al* 2011 Point design targets, specifications, and requirements for the 2010 ignition campaign on the National Ignition Facility *Phys. Plasmas* **18** 051001
[7] Remington B A *et al* 2019 Rayleigh–Taylor instabilities in high-energy density settings on the National Ignition Facility *Proc. Natl Acad. Sci. USA* **116** 18233
[8] Drake R P 2009 Perspectives on high-energy-density physics *Phys. Plasmas* **16** 055501
[9] Lugomer S 2016 Laser-matter interactions: inhomogeneous Richtmyer–Meshkov and Rayleigh–Taylor instabilities *Laser Part. Beams* **34** 123
[10] Mahalov A 2014 Multiscale modeling and nested simulations of three-dimensional ionospheric plasmas *Phys. Scr.* **89** 098001
[11] Wu P K, Kirkendall K A, Fuller R P and Nejad A S 1997 Breakup processes of liquid jets in subsonic crossows *J Prop Power* **13** 64–73
[12] Zeldovich Y B and Raizer Y P 2002 *Physics of Shock Waves and High-temperature Hydrodynamic Phenomena* 2nd edn (New York: Dover)
[13] Peters N 2000 *Turbulent Combustion.* (Cambridge: Cambridge University Press)
[14] Zhakhovsky V V, Kryukov A P, Levashov V Y, Shishkova I N and Anisimov S I 2019 Mass and heat transfer between evaporation and condensation surfaces *Proc Natl Acad Science USA* **116** 18209
[15] Buehler M J, Tang H, van Duin A C T and Goddard W A 2007 Threshold Crack Speed Controls Dynamical Fracture of Silicon Single Crystals *Phys. Rev. Lett.* **99** 165502
[16] Ilyin D V, Goddard W A III, Oppenheim J J and Cheng T 2019 First-principles–based reaction kinetics from reactive molecular dynamics simulations: Application to hydrogen peroxide decomposition *Proc. Natl Acad. Sci. USA* **116** 18202

[17] van Duin A C T, Dasgupta S, Lorant F and Goddard W A 2001 ReaxFF: a reactive force field for hydrocarbons *J. Phys. Chem.* A **105** 9396–409
[18] Anisimov S I, Drake R P, Gauthier S, Meshkov E E and Abarzhi S I 2013 What is certain and what is not so certain in our knowledge of Rayleigh–Taylor mixing? *Phil. Trans. R. Soc.* A **371** 20130266
[19] Abarzhi S I 2010 Review of theoretical modeling approaches of Rayleigh-Taylor instabilities and turbulent mixing *Phil. Trans. R. Soc.* A **368** 1809–28
[20] Landau L D and Lifshitz E M 1987 *Theory Course I-X* (New York: Pergamon)
[21] Abarzhi S I, Ilyin D V, Goddard W A III and Anisimov S 2019 Interface dynamics: new mechanisms of stabilization and destabilization and structure of flow fields *Proc. Natl Acad. Sci. USA* **116** 18218
[22] Ilyin D V, Fukumoto Y, Goddard W A and Abarzhi S I 2018 Analysis of dynamics, stability, and flow fields' structure of an accelerated hydrodynamic discontinuity with interfacial mass flux by a general matrix method *Phys. Plasmas* **25** 112105
[23] Abarzhi S I, Fukumoto Y and Kadanoff L P 2015 Stability of a hydrodynamic discontinuity *Phys. Scr.* **90** 018002
[24] Rayleigh L 1883 Investigations of the character of the equilibrium of an incompressible heavy fluid of variable density *Proc London Math Soc* **14** 170–7
[25] Taylor G I 1950 The instability of liquid surfaces when accelerated in a direction perpendicular to their planes *Proc. R. Soc. London* A **201** 192–6
[26] Richtmyer R D 1960 Taylor instability in shock acceleration of compressible fluids *Commun. Pure Appl. Math.* **13** 297–319
[27] Meshkov E E 1969 Instability of the interface of two gases accelerated by a shock *Sov Fluid Dyn* **4** 101–4
[28] Meshkov E E and Abarzhi S I 2019 On Rayleigh-Taylor interfacial mixing *Fluid Dyn. Res.* **51** 065502
[29] Abarzhi S I, Bhowmick A K, Naveh A, Pandian A, Swisher N C, Stellingwerf R F and Arnett W D 2019 Supernova, nuclear synthesis, fluid instabilities and mixing *Proc. Natl Acad. Sci. USA* **116** 18184
[30] Chandrasekhar S 1981 *Hydrodynamic and Hydromagnetic Stability*. (New York: Dover)
[31] Nishihara K, Wouchuk J G, Matsuoka C, Ishizaki R and Zhakhovsky V V 2010 Richtmyer–Meshkov instability: theory of linear and nonlinear evolution *Phil. Trans. R. Soc.* A **368** 1769–807
[32] Landau L D 1944 On the theory of slow combustion *Acta Physicochim URSS* **19** 77–85
[33] Class A G, Matkowsky B J and Klimenko A Y 2003 Stability of planar flames as gas-dynamic discontinuities *J. Fluid Mech.* **491** 51–63
[34] Sivashinsky G I 1983 Instabilities, pattern formation, and turbulence in flames *Ann Rev Fluid Mech* **15** 179–99
[35] Prosperetti A 2017 Vapor bubbles *Annual Review of Fluid Mechanics* **49** 221–48
[36] Bodner S E 1974 Rayleigh–Taylor instability and laser-pellet fusion *Phys. Rev. Lett.* **33** 761–4
[37] Kull H J and Anisimov S I 1986 Ablative stabilization in the incompressible Rayleigh–Taylor instability *Phys. Fluids* **29** 2067
[38] Sanz J 1994 Self-consistent analytical model of the Rayleigh-Taylor instability in inertial confinement fusion *Phys.Rev.Lett.* **73** 2700–3
[39] Aglitskiy Y *et al* 2010 Basic hydrodynamics of Richtmyer–Meshkov-type growth *Phil. Trans. R. Soc.* A **368** 1739–68
[40] Azechi H, Sakaiya T, Fujioka S, Tamari Y, Otani K, Shigemori K, Nakai M, Shiraga H, Miyanaga N and Mima K 2007 Comprehensive diagnosis of growth rates of the ablative Rayleigh-Taylor instability *Phys. Rev. Lett.* **98** 045002
[41] Kadau K, Barber J L, Germann T C, Holian B L and Alder B J 2010 Atomistic methods in fluid simulation *Phil. Trans. R. Soc.* A **368** 1547
[42] Karthik K, Dominic K and Herrmann M 2018 An in-cell reconstruction finite volume method for flows of compressible immiscible fluids *J Comp Physics* **373** 784–810
[43] Glimm J, Lin X L, Liu Y and Zhao N 2001 Conservative front tracking and level set algorithms *Proc. Natl Acad. Sci. USA* **98** 14198–201
[44] D'yakov S P 1954 Ob ustoichivosti udarnyh voln *Zh Exp Teor Fiz* **27** 288–95 (in Russian)
[45] Kontorovich V M 1958 Concerning the stability of shock waves *Sov. Phys. JETP* **6** 1179–80
[46] Ilyin D V, Goddard W A III and Abarzhi S I 2020 Inertial dynamics of an interface with interfacial mass flux: stability and flow fields' structure, inertial stabilization mechanism, degeneracy of Landau's solution, effect of energy fluctuations, and chemistry-induced instabilities *Phys. Fluids* **32** 082105
[47] Clay Institute 2000 Millennium Problems https://claymath.org/millennium-problems
[48] Physica Scripta 2020 Focus Issue '10th Anniversary Program Turbulent Mixing and Beyond' Physica Scripta https://iopscience.iop.org/journal/1402-4896/page/Focus-Issue-on-10th-Anniversary-Program-Turbulent-Mixing-and-Beyond-TMB-2017
[49] The Noble Prize https://www.nobelprize.org/
[50] Physica Scripta 2014 Highlights https://cms.iopscience.org/1f7ae43f-cefe-11e4-a30d-29411a5deefe/PhysicaScripta-highlights.pdf?guest=true
[51] Davies R M and Taylor G I 1950 The mechanics of large bubbles rising through extended liquids and through liquids in tubes *Proc R Soc* A **200** 375–90
[52] Meshkov E E 2013 Some peculiar features of hydrodynamic instability development *Phil. Trans. R. Soc.* A **371** 20120288
[53] Robey H F, Zhou Y, Buckingham A C, Keiter P, Remington B A and Drake R P 2003 The time scale for the transition to turbulence in a high Reynolds number, accelerated flow *Phys. Plasmas* **10** 614
[54] Cross M C and Hohenberg P C 1993 Pattern formation outside of equilibrium *Rev. Mod. Phys.* **65** 851
[55] Abarzhi S I 2008 Review of nonlinear dynamics of the unstable fluid interface: conservation laws and group theory *Phys. Scr.* **2008** 014012
[56] Abarzhi S I and Rosner R 2010 Comparative study of approaches for modeling Rayleigh-Taylor turbulent mixing *Phys. Scr.* **T142** 014012
[57] Akula B, Suchandra P and Ranjan D 2017 Dynamics of unstably stratified free shear flows: an experimental investigation of coupled Kelvin–Helmholtz and Rayleigh–Taylor instability *J Fluid Mechanics* **816** 619 - 660
[58] Youngs D L 2013 The density ratio dependence of self-similar Rayleigh–Taylor mixing *Phil. Trans. R. Soc.* A **371** 20120173
[59] Dimonte G *et al* 2004 A comparative study of the turbulent Rayleigh-Taylor instability using high-resolution three-dimensional numerical simulations: The Alpha-Group collaboration *Phys. Fluids* **16** 1668–93
[60] Thornber B *et al* 2017 Late-time growth rate, mixing, and anisotropy in the multimode narrowband Richtmyer–Meshkov instability: the θ-group collaboration *Phys. Fluids* **29** 105107
[61] Waters in the Pacific and Atlantic oceans meet and do not mix, and the interface between the miscible fluids is globally stable https://pinterest.com/pin/202380576990469741/
[62] Gekelman W, Tang S W, Haas T D, Vincena S, Pribyl P and Sydora R 2019 Spiky electric and magnetic field structures in flux rope experiments *Proc. Natl Acad. Sci. USA* **116** 18239
[63] Liang Z, Bu W, Schweighofer K J, Walwark D J Jr, Harvey J S, Hanlon G R, Amoanu D, Erol C, Benjamin I and Schlossman M L 2019 Nanoscale view of assisted ion transport across the liquid–liquid interface *Proc. Natl Acad. Sci. USA* **116** 18227